

Boundary Element and Finite Element Coupling for Aeroacoustics Simulations

Nolwenn Balin¹, Fabien Casenave^{1,2}, François Dubois³,
Eric Duceau¹, Stefan Duprey^{1,4}, Isabelle Terrasse¹

¹ Airbus Group Innovations, 12 Rue Pasteur, 92150 Suresnes, France

² Université Paris-Est, CERMICS (ENPC), 6-8 Avenue Blaise Pascal, Cité Descartes,
F-77455 Marne-la-Vallée, France

³ CNAM, Laboratoire LMSSC, 292 rue Saint-Martin, 75141 Paris Cedex 03, France

⁴ Institut Elie Cartan, Université Henri Poincaré, 24-30 rue Lionnois, 54003 Nancy Cedex, France

April 2, 2015

Abstract

We consider the scattering of acoustic perturbations in a presence of a flow. We suppose that the space can be split into a zone where the flow is uniform and a zone where the flow is potential. In the first zone, we apply a Prandtl–Glauert transformation to recover the Helmholtz equation. The well-known setting of boundary element method for the Helmholtz equation is available. In the second zone, the flow quantities are space dependent, we have to consider a local resolution, namely the finite element method. Herein, we carry out the coupling of these two methods and present various applications and validation test cases. The source term is given through the decomposition of an incident acoustic field on a section of the computational domain’s boundary.

1 Introduction

Acoustics is a well known science and the basics mechanical and thermodynamical notions are well understood since the 19th century as shown *e.g.* with the classical books of Lord Rayleigh [43]. For a modern presentation of various aspects of this science, we refer to Morse and Ingard [38] and to the contribution of Bruneau *et al.* [13]. Acoustics can be presented with temporal or harmonic dynamics. In the first case, acoustics can be viewed as a hyperbolic problem and in the second, the Helmholtz equation plays a central role.

With direct numerical time integration, finite differences are naturally popular. Even if it has not been created for acoustics applications, the “Marker And Cell” method with staggered grids of Harlow and Welch [31] can be used very easily in acoustics. We refer also to the pioneering work of Virieux for geophysics applications [50]. A finite difference method uses a finite grid in a domain of finite size. How to express that waves can go outside the computational domain without reflection ? One possible solution is to derive appropriate absorbing boundary conditions (see *e.g.* the book of Taflove summarized [49]). Another possibility is to add a layer of absorbing material. Efficient absorbing layers have been first proposed for the vectorial wave equation (Maxwell in electromagnetism) by Bérenger [8], then applied in acoustics (scalar equation) by Abarbanel *et al.* [1]. It was adapted by our group for advective acoustics and staggered grids [26]. However, the adaptation of cartesian finite differences to complex industrial geometries is a very difficult task and other numerical methods have been developed in order to guarantee this flexibility. The finite element method is the most popular in this direction. We refer to the fundamental book of Zienkiewicz [53] essentially for structural mechanics applications and to Craggs [20] for the acoustics applications. A rigorous mathematical analysis of the method with Hilbertian mathematical methods is proposed in the book of Ciarlet [18]. The main advantages of these so-called volume methods is the possibility to deal with space dependent media of propagation.

When the medium of propagation is uniform, the opportunity to represent the field as an integral representation over a surface of some data on the boundary of the radiating object makes natural so-called integral methods. The unknown is a field simply located on a finite surface and the three-dimensional field couples all the degrees of freedom on the surface. The difficulty is to take into account the fact that waves are radiating from finite distance towards infinity. The radiation Sommerfeld condition solves this problem and expresses that no wave is coming from infinity [47]. The adaptation of these ideas to integral methods for exterior boundary-value problems for Helmholtz equation have been discussed among others by Schenck [46] and Burton and Miller [14]. For a rigorous mathematical analysis, we refer to Nédélec [41]. The main advantages of these so-called integral methods is the possibility to deal with large geometries. In particular, in the case of the scattering by two objects, the size of the numerical problem does not depend on the distance between the objects. Besides, we have access to the scattered field at any point of the space.

A natural idea to profit from the advantages of volume and integral methods is the coupling between boundary and finite element methods. The fundamental mathematical work is due to Zienkiewicz, Kelly, and Bettess [53], Johnson and Nédélec [32], and Costabel [19]. The thesis of Levillain [34] gives the first numerical applications for Maxwell equations. We refer to Bielak and Mac Camy [9] for fluid - solid coupling. For other modern developments, we refer to the work of Abboud *et al.* (see *e.g.* [2]).

Integral methods have been implemented using Boundary Element Method (BEM) at former Airbus Research Center at Suresnes and Toulouse (France) since 2001 [21, 22] and used by Airbus first for computation of radiated noise outside air inlet than exhaust with the assumption of uniform flow on whole domain [23].

Several improvements have then been conducted by our team in two main ways : (i) increasing the number of unknowns - leading to the computation of the acoustic propagation at higher frequencies - using efficient numerical method such as the Fast Multipole Method [48, 29]; (ii) increasing the complexity of the flow to deal with more realistic problems. First results for coupled BEM-FEM with a uniform flow at infinity and potential flow assumption close to the scattering object have been obtained in an axisymmetric configuration in [27]. Mathematical framework in the 3D case have been presented in [16]. In this contribution, we present an extension of the previous works in a more general context closer to applications and taking into account realistic air inlets: our main objective is to perform a global simulation from a given Mach number in the duct to a different Mach number in far field with a transitional potential flow between the two zones.

The model coupled problem is presented in Section 2. This problem is transformed by the Prandtl-Glauert transformation, in order to recover the classical Helmholtz equation in the area where the flow is uniform in Section 3, leading to a transformed coupled weak formulation. The finite dimensional linear system is presented in Section 4, and numerical studies are carried out in Section 5.

2 Definition of the model problem

2.1 Context and geometry

The objective of the current work is the computation of the acoustic field generated by a turboreactor engine in flight condition, especially in take-off and landing phases. We will consider the model problem presented in Figure 1, where the other parts of the aircraft (engine pylon, wings, fuselage) are not modeled.

The considered acoustic sources are the inward and outward fans noise. The fan noise frequency spectrum is characterized by some harmonic peaks at frequencies that are multiple of the rotational frequency of the blades. For simplicity, we consider a single pulsation ω_0 . Moreover, the fans are located inside a duct that is relatively deep compared to its width. For these reasons, it is classical to model the duct by semi-infinite cylinders, and represent the acoustic sources on modal bases functions defined at the bases of these cylinders, called modal surfaces. As illustrated on Figure 1, two modal surfaces Γ_{M_1} and Γ_{M_2} are defined. The other part of the engine boundary is rigid and noted Γ .

The complexity of the flow depends on the distance from the engine. For low Mach values, the flow can be decomposed into three areas with different flow conditions: a uniform flow far from the

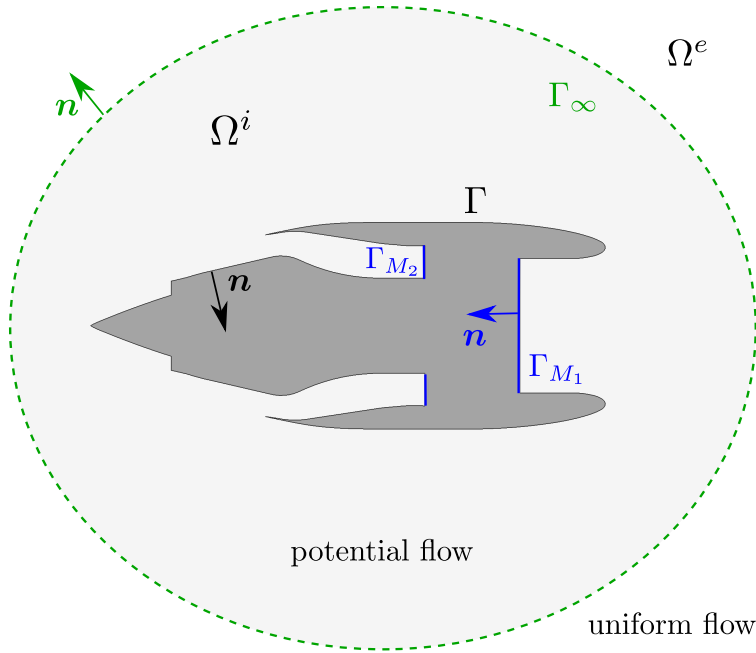


Figure 1: Model problem (without representation of the fan spinner)

engine, a turbulent flow (often non-linear) due to the fans and the boundary layers, and a potential flow in-between. We use this decomposition in our model, except for the turbulent area.

Some other models such as the Galbrun equation [11] could also be considered in order to take into account the influence of some rotational flow on the acoustic propagation. The impact of the viscosity effect and in particular the boundary layers is neglected in this contribution. This assumption is classical in the community of industrial acoustics. In air intake cases (see *e.g.* Lidoine [35]), there is no flow separation. The boundary layer remains very thin compared to the wavelength of interest and is not taken into account for the acoustic point of view. The problem of thin boundary layers in the duct flow has been studied by Eversman [28]. This question has been emphasized after the work of Myers [40]. The Myers boundary condition has been improved by Brambley [12]. For an ejection duct, the situation is more complicated because anyway the flow is far from potential. In particular, a mixing layer containing different jets is present. Moreover, its thickness is small near the ejection compared to the characteristics lengths of the problem. As a consequence, it is reasonable to assume that the sound has a negligible influence on the flow.

The interior part of the engine is also supposed to be behind the modal surfaces. We then consider only two domains: Ω^i with a potential flow and Ω^e with a uniform flow. The flow is an input to the problem. Matching conditions on the flow are supposed at the interface Γ_∞ between these two domains. Moreover, at Γ_{M_1} and Γ_{M_2} , the flow is supposed uniform and orthogonal to the surface. It is also tangent to Γ .

2.2 Coupled problem

2.2.1 Convected Helmholtz equation

For simplicity, only one modal surface Γ_M is considered in the model problem instead of Γ_{M_1} and Γ_{M_2} as presented on Figure 1. We define Ω^M as a semi-infinite waveguide with base Γ_M and oriented along the axis of the engine, see Figure 2.

We note c_0 the speed of sound, ρ_0 the density, \mathbf{M}_0 the Mach vector of the fluid defined in Ω^i . We suppose that these quantities are continuous over $\Omega^i \cup \Gamma_\infty \cup \Gamma_M$ and extend them such that

$$\begin{aligned} \forall \mathbf{x} \in \Gamma_\infty : & \quad c_0(\mathbf{x}) = c_\infty, & \quad \rho_0(\mathbf{x}) = \rho_\infty, & \quad \mathbf{M}_0(\mathbf{x}) = \mathbf{M}_\infty, \\ \forall \mathbf{x} \in \Gamma_M : & \quad c_0(\mathbf{x}) = c_M, & \quad \rho_0(\mathbf{x}) = \rho_M, & \quad \mathbf{M}_0(\mathbf{x}) = \mathbf{M}_M. \end{aligned}$$

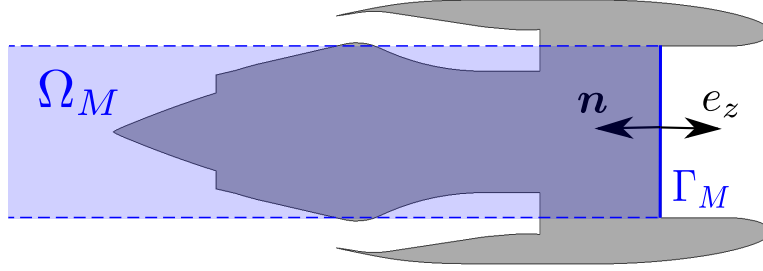


Figure 2: Model of the engine : a semi-infinite waveguide.

Notice that c_0 , ρ_0 and \mathbf{M}_0 denote respectively the point-dependent speed of sound, density and Mach number vector field in the open domain Ω^i . The quantities c_∞ and c_M , ρ_∞ and ρ_M , \mathbf{M}_∞ and \mathbf{M}_M are constant and defined as limit values of c_0 , ρ_0 and \mathbf{M}_0 on respectively the boundaries Γ_∞ and Γ_M .

We note \mathbf{v} and p the acoustic velocity and pressure, defined in Ω^i as well.

In the interior domain Ω^i , the convective flow is supposed to be subsonic, stationary, non viscous, isentropic, and irrotational. Moreover, the acoustic effects are considered to be a first order perturbation of this flow. With these assumptions, the acoustic velocity \mathbf{v} is potential. Hence, there exists an acoustic potential, φ , such that $\mathbf{v} = \nabla\varphi$. We note by φ^e and φ^i the acoustic potential respectively restricted to Ω^e and Ω^i .

The physical quantities are associated with complex quantities with the following convention on, for instance, the acoustic potential: $\varphi \leftrightarrow \Re(\varphi \exp(-i\omega_0 t))$. The same notation is taken for the physical quantity and its complex counterpart. In what follows, we always refer to the complex quantities. The wavenumber depends on the position in Ω^i . From the continuity of c_0 over $\Omega^i \cup \Gamma_\infty \cup \Gamma_M$, we can define

$$k_0(\mathbf{x}) = k_\infty := \frac{\omega_0}{c_\infty} \quad \forall \mathbf{x} \in \Gamma_\infty, \quad k_0(\mathbf{x}) = k_M := \frac{\omega_0}{c_M} \quad \forall \mathbf{x} \in \Gamma_M.$$

Following [45, p.259 eq.F27], and making use of the irrotationality of the carrier flow, the linearization of the Euler equations leads to

$$\mathcal{H}(\varphi) = 0 \quad \text{in } \Omega^i \cup \bar{\Omega}^e, \quad (1)$$

where $\mathcal{H}(\varphi) := \rho_0 (k_0^2 \varphi + ik_0 \mathbf{M}_0 \cdot \nabla \varphi) + \text{div} [\rho_0 (\nabla \varphi - (\mathbf{M}_0 \cdot \nabla \varphi) \mathbf{M}_0 + ik_0 \varphi \mathbf{M}_0)]$. This is the convected Helmholtz equation. We assume that Γ reflects perfectly the acoustic perturbations, yielding

$$\nabla \varphi \cdot \mathbf{n} = 0 \quad \text{on } \Gamma. \quad (2)$$

We now explain how the problem in Ω^i is coupled to a problem in Ω^e and a problem beyond Γ_M by means of boundary conditions on Γ_∞ and Γ_M .

2.2.2 Coupling by means of boundary conditions

To focus on the coupling between the problem in Ω^i and the one in Ω^e , consider a test case like the one Figure 1, where some boundary condition is enforced on Γ_M :

$$\left\{ \begin{array}{ll} \mathcal{H}(\varphi) = 0, & \text{in } \Omega^i \cup \Gamma_\infty \cup \Omega^e, \\ \nabla \varphi \cdot \mathbf{n} = 0, & \text{on } \Gamma, \\ \varphi = g, & \text{on } \Gamma_M, \\ \text{Sommerfeld radiation condition,} & \end{array} \right. \quad (3)$$

where a Sommerfeld-like radiation condition is enforced to ensure uniqueness of problem by selecting outgoing scattered waves and where g is some nonzero function defined on Γ_M . Consider the following

problem

$$\left\{ \begin{array}{ll} \mathcal{H}(\varphi) = 0, & \text{in } \Omega^i, \\ \mathcal{H}(\varphi) = 0, & \text{in } \Omega^e, \\ [\varphi]_{\Gamma_\infty} = 0, & \text{on } \Gamma_\infty, \\ [(\nabla\varphi - (\mathbf{M}_\infty \cdot \nabla\varphi) \mathbf{M}_\infty + ik_\infty\varphi\mathbf{M}_\infty) \cdot \mathbf{n}]_{\Gamma_\infty} = 0, & \text{on } \Gamma_\infty, \\ \nabla\varphi \cdot \mathbf{n} = 0, & \text{on } \Gamma, \\ \varphi = g, & \text{on } \Gamma_M, \\ \text{Sommerfeld-like radiation condition,} & \end{array} \right. \quad (4)$$

where $[\cdot]_X$ denotes the jump of a quantity across a surface X . In Equation (4), the coupling conditions are written before the Prandtl–Glauert transformation is performed, unlike in [16] where the Prandtl–Glauert transformation is performed beforehand. The two formulations lead to the same result.

Property 2.1. *Problems 3 and 4 are equivalent.*

Proof. If φ solves (3), it is clear that φ solves (4). Conversely, let φ defined in $\Omega^i \cup \Omega^e$ such that φ verifies (4). From [36, Lemma 4.19], since φ verifies lines 1, 2, 3, 4 of (4), then φ verifies line 1 of (3), which finishes the proof. \square

Using the transmission conditions of problem (4) on Γ_∞ , we will write problem (3) in the form of a problem on φ^i and a boundary condition on Γ_∞ . Consider the following problem in Ω^e

$$\left\{ \begin{array}{ll} \mathcal{H}(\varphi^e) = 0, & \text{in } \Omega^e, \\ \varphi^e = F, & \text{on } \Gamma_\infty, \\ \text{Sommerfeld-like radiation condition,} & \end{array} \right. \quad (5)$$

where F is some nonzero function on Γ_∞ . With some regularity hypothesis on Ω^e and F , problem (5) has a unique solution in $H_{\text{loc}}^1(\Omega^e)$, where $H_{\text{loc}}^1(\Omega^e) := \{u \in H^1(K), \forall K \subset \Omega^e \text{ compact}\}$, [36, Theorem 9.11].

Remark 2.1. [36, Theorem 9.11] deals with the classical Helmholtz equations. We will see in Section 3 that the classical Helmholtz equation can be obtained from the convected Helmholtz equation applying a certain transformation. In particular, the solution functions are changed by an injective transformation, ensuring existence and uniqueness of problem (5).

Thus, it is possible to define the operator that maps F onto $(\nabla\varphi^e - (\mathbf{M}_\infty \cdot \nabla\varphi^e) \mathbf{M}_\infty + ik_\infty\varphi^e\mathbf{M}_\infty)|_{\Gamma_\infty} \cdot \mathbf{n}$, where φ^e is the solution of problem (5). This operator is called the Dirichlet-to-Neumann operator associated with the exterior problem (5), and is denoted by Λ_∞ . Hence, problem (3) is written

$$\left\{ \begin{array}{ll} \mathcal{H}(\varphi^i) = 0, & \text{in } \Omega^i, \\ (\nabla\varphi^i - (\mathbf{M}_\infty \cdot \nabla\varphi^i) \mathbf{M}_\infty + ik_\infty\varphi^i\mathbf{M}_\infty) \cdot \mathbf{n} = \Lambda_\infty(\varphi^i), & \text{on } \Gamma_\infty, \\ \nabla\varphi^i \cdot \mathbf{n} = 0, & \text{on } \Gamma, \\ \varphi^i = g, & \text{on } \Gamma_M. \end{array} \right. \quad (6)$$

The same reasoning is done on Γ_M , the following transmission condition holds: $[\varphi]_{\Gamma_M} = 0$ and $[(\nabla\varphi - (\mathbf{M}_M \cdot \nabla\varphi) \mathbf{M}_M + ik_M\varphi\mathbf{M}_M) \cdot \mathbf{n}]_{\Gamma_M} = 0$. Then, we write a coupled problem between Ω^i and Ω^M . The acoustic problem in Ω_M with a Dirichlet boundary condition on Γ_M is well-posed, so that a Dirichlet-to-Neumann operator associated with the problem in Ω_M can be defined, and is denoted by Λ_M . Hence, using the transmission conditions on Γ_M , the boundary condition at Γ_M of the interior problem is $(\nabla\varphi^i - (\mathbf{M}_M \cdot \nabla\varphi^i) \mathbf{M}_M + ik_M\varphi^i\mathbf{M}_M) \cdot \mathbf{n}|_{\Gamma_M} = \Lambda_M(\varphi^i|_{\Gamma_M})$.

2.2.3 Weak formulation

Finally, the complete coupled problem is written

$$\left\{ \begin{array}{ll} \mathcal{H}(\varphi^i) = 0, & \text{in } \Omega^i, \\ \nabla \varphi^i \cdot \mathbf{n} = 0, & \text{on } \Gamma, \\ (\nabla \varphi^i - (\mathbf{M}_\infty \cdot \nabla \varphi^i) \mathbf{M}_\infty + ik_\infty \varphi^i \mathbf{M}_\infty) \cdot \mathbf{n} = \Lambda_\infty(\varphi^i), & \text{on } \Gamma_\infty, \\ (\nabla \varphi^i - (\mathbf{M}_M \cdot \nabla \varphi^i) \mathbf{M}_M + ik_M \varphi^i \mathbf{M}_M) \cdot \mathbf{n} = \Lambda_M(\varphi^i), & \text{on } \Gamma_M. \end{array} \right. \quad (7)$$

The weak formulation of the coupled problem is: Find $\varphi^i \in H^1(\Omega^i)$ such that $\forall \varphi^t \in H^1(\Omega^t)$,

$$a(\varphi^i, \varphi^t) + I_\infty(\varphi^i, \varphi^t) + I_M(\varphi^i, \varphi^t) = 0, \quad (8)$$

with

$$a(\varphi^i, \varphi^t) = \int_{\Omega^i} \frac{\rho_0}{\rho_\infty} \left[\nabla \varphi^i \cdot \nabla \overline{\varphi^t} - k_0^2 \varphi^i \overline{\varphi^t} - ik_0 \left((\mathbf{M}_0 \cdot \nabla \varphi^i) \overline{\varphi^t} - (\mathbf{M}_0 \cdot \nabla \overline{\varphi^t}) \varphi^i \right) - (\mathbf{M}_0 \cdot \nabla \varphi^i) (\mathbf{M}_0 \cdot \nabla \overline{\varphi^t}) \right], \quad (9)$$

$$I_\infty(\varphi^i, \varphi^t) = - \int_{\Gamma_\infty} \Lambda_\infty(\varphi^i) \overline{\varphi^t}, \quad (10)$$

$$I_M(\varphi^i, \varphi^t) = - \frac{\rho_M}{\rho_\infty} \int_{\Gamma_M} \Lambda_M(\varphi^i) \overline{\varphi^t}. \quad (11)$$

The Λ_∞ map can be expressed by means of boundary integral operators written on Γ_∞ . The problem in the exterior domain depends on \mathbf{M}_∞ . The next step is to transform (8) in such a way that the problem in the exterior domain becomes the classical Helmholtz solution. This is of great interest, since we already dispose of a code evaluating the classical boundary integral operators for the classical Helmholtz equation.

3 Transformation of the coupled problem

The purpose of this section is to apply a transformation to the weak formulation (8), such that the Λ_∞ map can be expressed in a convenient way. The expression of Λ_M resulting of the transformation is also given, to obtain a complete transformed coupled formulation written in the same system of coordinates.

3.1 Prandtl–Glauert transformation

When the carrier flow is at rest, the acoustic potential φ^e is solution of the Helmholtz equation. The Prandtl–Glauert transformation was introduced by Glauert in 1928 in [30], to study the compressible effects of the air on the lift of an airfoil. This transformation was applied for subsonic aeroacoustics problems by Amiet and Sears in [5] in 1970, by Astley and Bain [6] and more recently by our team in 2002 in [26].

Definition 3.1. *The Prandtl–Glauert transformation associated to \mathbf{M}_∞ consists in changing the space and time variables:*

$$\left\{ \begin{array}{l} \tilde{\mathbf{x}} = \mathbf{x} + C_\infty (\mathbf{M}_\infty \cdot \mathbf{x}) \mathbf{M}_\infty, \\ \tilde{t} = t + \frac{\gamma_\infty^2}{c_\infty} \mathbf{M}_\infty \cdot \mathbf{x}, \end{array} \right. \quad (12)$$

where $C_\infty = \frac{1}{M_\infty^2} (\gamma_\infty - 1)$, with $\gamma_\infty = \frac{1}{\sqrt{1 - M_\infty^2}}$.

We define the spatial transformation L :

$$\mathbb{R}^3 \ni \mathbf{x} \rightarrow L(\mathbf{x}) := \tilde{\mathbf{x}} \in \mathbb{R}^3. \quad (13)$$

The transformation $L_{|\Omega^i}$ is a dilatation of magnitude γ_∞ along \mathbf{M}_∞ . Denote J_∞ the jacobian of $L_{|\Omega^i}^{-1}$, the inverse of this transformation. Consider an orthonormal basis $(\mathbf{x}', \mathbf{y}', \mathbf{z}')$ of \mathbb{R}^3 so that $\mathbf{z}' = \frac{\mathbf{M}_\infty}{M_\infty}$. In this basis, the jacobian matrix of $L_{|\Omega^i}^{-1}$ is

$$\begin{pmatrix} 1 & 0 & 0 \\ 0 & 1 & 0 \\ 0 & 0 & \gamma_\infty^{-1} \end{pmatrix}, \quad (14)$$

so that $J_\infty = \gamma_\infty^{-1}$.

From [51, Section 10.3.1], applying the Prandtl–Glauert transformation, the transformed acoustic potential in the exterior domain f^e satisfies

$$\tilde{\Delta} f^e + \tilde{k}_\infty^2 f^e = 0, \quad \text{in } \tilde{\Omega}^e, \quad (15)$$

where $\tilde{k}_\infty := \gamma_\infty k_\infty$ is the modified wavenumber. This is a classical Helmholtz equation. The Sommerfeld radiation condition

$$\tilde{r} \left(\frac{\partial f^e}{\partial \tilde{r}} - i \tilde{k}_\infty f^e \right) \rightarrow 0, \quad \tilde{r} \rightarrow +\infty \quad (16)$$

is enforced as well to ensure uniqueness of the solution [47].

Remark 3.1 (Coordinate transformations). *Other coordinate transformations can retrieve the classical Helmholtz equation from the uniformly convected Helmholtz equation. For instance, Lorentz-like transformations are possible, but would lead to frequency dependent meshes, which is not desirable. The coordinate transformation (12) we used belongs to a general family of transformations proposed in [17]. With (12), the flux of the Poynting vector is conserved through any surface orthogonal to \mathbf{M}_∞ .*

Remark 3.2. *We define a Prandtl–Glauert transformation associated to another vector \mathbf{v} by changing \mathbf{M}_∞ and M_∞ by respectively \mathbf{v} and $\|\mathbf{v}\|$ in Definition 3.1. In what follows, we note by $\tilde{\cdot}$ the objects and operators transformed by the Prandtl–Glauert transformation associated to \mathbf{M}_∞ (normals, geometry, derivatives).*

3.2 Transformation of the volume integral term a (9)

In what follows, the Prandtl–Glauert transformation is carried-out in the interior domain after the weak formulation has been written. Doing so, the obtained formulation is written in a form that uses operators that are already implemented in the code ACTIPOLE [21, 22]. Another choice can be to carry out the Prandtl–Glauert transformation first, and then write the weak formulation. The two formulations are equivalent, but this last case suits well to the study of the existence and uniqueness of the formulation (see [16]).

Consider the solution function $\phi^i(t, \mathbf{x}) = \varphi^i(\mathbf{x}) e^{-i\omega t}$. Applying the Prandtl–Glauert transformation (12), this function transforms into $\varphi^i(L^{-1}(\tilde{\mathbf{x}})) e^{ik_\infty \gamma_\infty^2 \mathbf{M}_\infty \cdot L^{-1}(\tilde{\mathbf{x}})} e^{-i\omega \tilde{t}}$. This motivates the introduction of the function f^i , such that $f^i(\mathbf{x}) = \varphi^i(\mathbf{x}) \mathcal{E}_\infty(\mathbf{x})$, where $\mathcal{E}_\infty(\mathbf{x}) = e^{ik_\infty \gamma_\infty^2 \mathbf{M}_\infty \cdot \mathbf{x}}$. We define f^t from the test function φ^t in the same fashion. This leads to

$$\begin{aligned} \varphi^i(\mathbf{x}) &= f^i(\mathbf{x}) \overline{\mathcal{E}_\infty(\mathbf{x})} \\ \overline{\varphi^t(\mathbf{x})} &= \overline{f^t(\mathbf{x})} \mathcal{E}_\infty(\mathbf{x}). \end{aligned} \quad (17)$$

The transformation $H^1(\Omega^i) \ni \varphi^t(\mathbf{x}) \rightarrow f^t(\mathbf{x}) \mathcal{E}_\infty(\mathbf{x}) \in H^1(\Omega^i)$ is surjective, and therefore this modification of test functions is still compatible with the weak formulation. The gradients rewrite

$$\begin{aligned} \nabla \varphi^i(\mathbf{x}) &= (\nabla f^i(\mathbf{x}) - ik_\infty \gamma_\infty^2 \mathbf{M}_\infty f^i(\mathbf{x})) \overline{\mathcal{E}_\infty(\mathbf{x})} \\ \nabla \overline{\varphi^t(\mathbf{x})} &= \left(\nabla \overline{f^t(\mathbf{x})} + ik_\infty \gamma_\infty^2 \mathbf{M}_\infty \overline{f^t(\mathbf{x})} \right) \mathcal{E}_\infty(\mathbf{x}). \end{aligned} \quad (18)$$

Thus, Equation (9) becomes

$$a(\varphi^i, \varphi^t) = \int_{\Omega^i} \frac{\rho_0}{\rho_\infty} \left[(\mathcal{L}_- f^i) \cdot (\mathcal{L}_+ \bar{f}^t) - k_0^2 f^i \bar{f}^t - ik_0 \left((\mathbf{M}_0 \cdot (\mathcal{L}_- f^i)) \bar{f}^t - (\mathbf{M}_0 \cdot (\mathcal{L}_+ \bar{f}^t)) f^i \right) \right] - \int_{\Omega^i} \frac{\rho_0}{\rho_\infty} (\mathbf{M}_0 \cdot (\mathcal{L}_- f^i)) (\mathbf{M}_0 \cdot (\mathcal{L}_+ \bar{f}^t)), \quad (19)$$

where $\mathcal{L}_\pm := \nabla \pm ik_\infty \gamma_\infty^2 \mathbf{M}_\infty$ and where we used $\overline{\mathcal{E}_\infty(\mathbf{x})} \mathcal{E}_\infty(\mathbf{x}) = 1$.

Then, applying the change of variables and making use of the jacobian J_∞ of $L_{|\Omega^i}^{-1}$, there holds

$$a(\varphi^i, \varphi^t) = J_\infty \int_{\widetilde{\Omega}^i} \frac{\rho_0}{\rho_\infty} \left[(\widetilde{\mathcal{L}}_- f^i) \cdot (\widetilde{\mathcal{L}}_+ \bar{f}^t) - k_0^2 f^i \bar{f}^t - ik_0 \left((\mathbf{M}_0 \cdot (\widetilde{\mathcal{L}}_- f^i)) \bar{f}^t - (\mathbf{M}_0 \cdot (\widetilde{\mathcal{L}}_+ \bar{f}^t)) f^i \right) \right] - J_\infty \int_{\widetilde{\Omega}^i} \frac{\rho_0}{\rho_\infty} (\mathbf{M}_0 \cdot (\widetilde{\mathcal{L}}_- f^i)) (\mathbf{M}_0 \cdot (\widetilde{\mathcal{L}}_+ \bar{f}^t)), \quad (20)$$

where $\widetilde{\mathcal{L}}_\pm := \widetilde{\nabla} + (C_\infty \mathbf{M}_\infty \cdot \widetilde{\nabla} \pm ik_\infty \gamma_\infty^2) \mathbf{M}_\infty$. Notice that when changing the variables, we wrote the differential operators in the transformed system of coordination, using

$$\nabla \rightarrow \widetilde{\nabla} + C_\infty \mathbf{M}_\infty \mathbf{M}_\infty \cdot \widetilde{\nabla}, \quad (21)$$

which is directly derived from the first line of (12).

Remark 3.3. *If we impose $\mathbf{M}_0 = \mathbf{M}_\infty$, $\rho_0 = \rho_\infty$ and $c_0 = c_\infty$ in (20), we find*

$$a(\varphi^i, \varphi^t) = J_\infty \int_{\widetilde{\Omega}^i} \left(\widetilde{\nabla} f^i \cdot \widetilde{\nabla} \bar{f}^t - \widetilde{k}_\infty^2 f^i \bar{f}^t \right), \quad (22)$$

which is the variational formulation for the nonconvected Helmholtz equation with modified wavenumber $\widetilde{k}_\infty = \gamma_\infty k_\infty$ on f on the transformed geometry and in the transformed coordinates.

Remark 3.4. *The expression (20) for the volume integral is more complicated than the expression (9). However, this will enable us to treat the coupling with the exterior domain in a simple way.*

3.3 Transformation of the surface integral term I_∞ (10)

3.3.1 Transformation of normals

Consider \mathcal{C} , a subset of \mathbb{R}^3 defined by a function Φ by $\Phi(\mathbf{x}) = 0$, such that $\{x \in \mathcal{C}\}$ is a closed surface in \mathbb{R}^3 . Denote by $\widetilde{\mathcal{C}}$ the transformation of \mathcal{C} by L . Let $\mathbf{x} \in \mathcal{C}$, the normal to \mathcal{C} at \mathbf{x} , $\mathbf{n}(\mathbf{x})$, is colinear to $\nabla \Phi(\mathbf{x})$, whereas the normal to $\widetilde{\mathcal{C}}$ at $\widetilde{\mathbf{x}}$, $\widetilde{\mathbf{n}}(\widetilde{\mathbf{x}})$, is colinear to $\widetilde{\nabla} \Phi(\widetilde{\mathbf{x}})$. From (21), there then holds

$$\mathbf{n}(\mathbf{x}) = K_\infty(\widetilde{\mathbf{x}}) (\widetilde{\mathbf{n}}(\widetilde{\mathbf{x}}) + C_\infty (\mathbf{M}_\infty \cdot \widetilde{\mathbf{n}}(\widetilde{\mathbf{x}})) \mathbf{M}_\infty), \quad (23)$$

where $K_\infty(\widetilde{\mathbf{x}})$ is a normalization factor. Taking the square of the norm of both sides of (23), there holds $1 = K_\infty(\widetilde{\mathbf{x}})^2 \left(1 + (M_\infty^2 C_\infty^2 + 2C_\infty) (\mathbf{M}_\infty \cdot \widetilde{\mathbf{n}}(\widetilde{\mathbf{x}}))^2 \right)$, from which we deduce

$$K_\infty(\widetilde{\mathbf{x}}) = \sqrt{1 + (\gamma_\infty \mathbf{M}_\infty \cdot \widetilde{\mathbf{n}}(\widetilde{\mathbf{x}}))^2}. \quad (24)$$

Conversely, to express $\widetilde{\mathbf{n}}(\widetilde{\mathbf{x}})$ as a function of $\mathbf{n}(\mathbf{x})$, we consider the inverse spatial transformation L^{-1} , which consists of a contraction of magnitude γ_∞^{-1} along \mathbf{M}_∞ . The gradient are then changed as $\widetilde{\nabla} \rightarrow \nabla + \widetilde{C}_\infty \mathbf{M}_\infty \mathbf{M}_\infty \cdot \nabla$, where $\widetilde{C}_\infty = \frac{1}{M_\infty^2} (\gamma_\infty^{-1} - 1)$. Applying this to the gradient of $\Phi(\widetilde{\mathbf{x}}) = 0$, which defines $\widetilde{\mathcal{C}}$, we deduce

$$\widetilde{\mathbf{n}}(\widetilde{\mathbf{x}}) = \widetilde{K}_\infty(\mathbf{x}) \left(\mathbf{n}(\mathbf{x}) + \widetilde{C}_\infty (\mathbf{M}_\infty \cdot \mathbf{n}(\mathbf{x})) \mathbf{M}_\infty \right), \quad (25)$$

where $\widetilde{K}_\infty(\mathbf{x})$ is a normalization factor. Using the normalization condition,

$$\widetilde{K}_\infty(\mathbf{x}) = \frac{1}{\sqrt{1 - (\mathbf{M}_\infty \cdot \mathbf{n}(\mathbf{x}))^2}}. \quad (26)$$

3.3.2 Jacobian of the spatial transformation restricted to Γ_∞

Consider $L|_{\Gamma_\infty}$, the restriction of L to the 2-dimensional manifold Γ_∞ . Let $\mathbf{x} \in \Gamma_\infty$. Let $\mathbf{m}_1 := \frac{\mathbf{M}_\infty}{M_\infty}$, $\mathbf{m}_2 := \frac{\mathbf{n} - (\mathbf{m}_1 \cdot \mathbf{n})\mathbf{m}_1}{\|\mathbf{n} - (\mathbf{m}_1 \cdot \mathbf{n})\mathbf{m}_1\|}$ and \mathbf{m}_3 such that $(\mathbf{m}_1, \mathbf{m}_2, \mathbf{m}_3)$ is a direct orthonormal triplet. Let $N := \mathbf{n} \cdot \mathbf{m}_1$. By construction, $\mathbf{n} = N\mathbf{m}_1 + \sqrt{1 - N^2}\mathbf{m}_2$. Then, we define $\mathbf{t}_1 := -\sqrt{1 - N^2}\mathbf{m}_1 + N\mathbf{m}_2$ and $\mathbf{t}_2 := \mathbf{m}_3$, see Figure 3. It is direct to verify that $(\mathbf{t}_1, \mathbf{t}_2)$ is an orthonormal doublet, and that

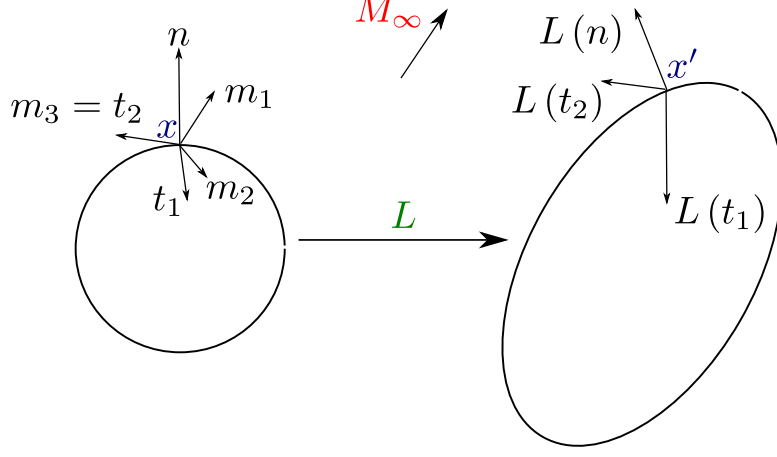


Figure 3: Transformation of a local basis on Γ_∞ by the Prandtl–Glauert transformation.

$\mathbf{t}_1 \cdot \mathbf{n} = \mathbf{t}_2 \cdot \mathbf{n} = 0$. Therefore, $(\mathbf{t}_1, \mathbf{t}_2)$ is an orthonormal basis for the hyperplane tangent to Γ_∞ in \mathbf{x} , and $|\text{Jac}(L|_{\Gamma_\infty})| = |\det(L(\mathbf{t}_1), L(\mathbf{t}_2))|$. Since we have identified in \mathbf{t}_1 and \mathbf{t}_2 the components parallel and orthogonal to \mathbf{M}_∞ , there holds $L(\mathbf{t}_1) = -\gamma_\infty \sqrt{1 - N^2}\mathbf{m}_1 + N\mathbf{m}_2$ and $L(\mathbf{t}_2) = \mathbf{t}_2 = \mathbf{m}_3$, because \mathbf{t}_2 is orthogonal to \mathbf{M}_∞ . We see that $L(\mathbf{t}_1)$ and $L(\mathbf{t}_2)$ are orthogonal, then $\det(L(\mathbf{t}_1), L(\mathbf{t}_2)) = \|L(\mathbf{t}_1)\| \|L(\mathbf{t}_2)\| = \|L(\mathbf{t}_1)\| = \sqrt{N^2 + \gamma_\infty^2(1 - N^2)} = \gamma_\infty \sqrt{1 - (\mathbf{M}_\infty \cdot \mathbf{n})^2}$, from which we deduce $|\text{Jac}(L|_{\Gamma_\infty}^{-1})| = J_\infty \widetilde{K}_\infty$.

3.3.3 Expression for I_∞

Consider equation (10) for I_∞ and use the boundary condition line 3 of (7):

$$I_\infty(\varphi^i, \varphi^t) = - \int_{\Gamma_\infty} (\nabla \varphi^i - (\mathbf{M}_\infty \cdot \nabla \varphi^i) \mathbf{M}_\infty - ik_\infty \varphi^i \mathbf{M}_\infty) \cdot \mathbf{n} \varphi^t. \quad (27)$$

Plugging the changes for order zero (17) and order one (18) terms and making use of the jacobian $\text{Jac}(L|_{\Gamma_\infty}^{-1})$, there holds

$$I_\infty(\varphi^i, \varphi^t) = -J_\infty \int_{\widetilde{\Gamma}_\infty} \widetilde{K}_\infty \left[(\widetilde{\nabla} f^i - ik_\infty \gamma_\infty \mathbf{M}_\infty f^i) \cdot (\mathbf{n} + (C_\infty - \gamma_\infty) (\mathbf{M}_\infty \cdot \mathbf{n}) \mathbf{M}_\infty) + ik_\infty f^i (\mathbf{M}_\infty \cdot \mathbf{n}) \right] \overline{f^t}. \quad (28)$$

Since $C_\infty - \gamma_\infty = \widetilde{C}_\infty$, we recognize the expression of $\frac{\widetilde{\mathbf{n}}}{\widetilde{K}_\infty}$. Reorganizing the terms:

$$I_\infty(\varphi^i, \varphi^t) = -J_\infty \int_{\widetilde{\Gamma}_\infty} \widetilde{\nabla} f^i \cdot \widetilde{\mathbf{n}} \overline{f^t} + J_\infty \int_{\widetilde{\Gamma}_\infty} ik_\infty f^i \left(\widetilde{K}_\infty (\mathbf{M}_\infty \cdot \mathbf{n}) - \gamma_\infty \mathbf{M}_\infty \cdot \widetilde{\mathbf{n}} \right) \overline{f^t}. \quad (29)$$

Finally, from relation (25), $\mathbf{M}_\infty \cdot \widetilde{\mathbf{n}} = \frac{\widetilde{K}_\infty}{\gamma_\infty} (\mathbf{M}_\infty \cdot \mathbf{n})$, and

$$I_\infty(\varphi^i, \varphi^t) = -J_\infty \int_{\widetilde{\Gamma}_\infty} \widetilde{\nabla} f^i \cdot \widetilde{\mathbf{n}} \overline{f^t}. \quad (30)$$

Remark 3.5. Notice the extreme simplification of the surface integral term (30). The direct coupling with the BEM is possible thanks to this particular form of the surface integral term. Notice also that (30) is simply the expression of the surface integral term of the weak formulation (8) after the Prandtl–Glauert transformation has been applied.

We now need to apply the Prandtl–Glauert transformation in the equation on the exterior domain Ω^e and we will see that (30) can be expressed using the Dirichlet-to-Neumann operator associated to the classical Helmholtz equation.

3.4 Derivation of the transformed $\widetilde{\Lambda}_\infty$ map

The derivation of a Dirichlet-to-Neumann map Λ_∞ for the Helmholtz exterior problem (15) is classical. The procedure is detailed for instance in [16]. We recall the main steps for completeness of the presentation. A function is called a radiating Helmholtz solution, if it solves the classical Helmholtz solution in Ω^e and in $\mathbb{R}^3 \setminus \overline{\Omega^e}$, and if it satisfies the Sommerfeld radiation condition. A radiating Helmholtz solution v can be represented from the jump of its traces on Γ [41, Theorem 3.1.1]

$$v = -\mathcal{S}[\nabla v \cdot \mathbf{n}] + \mathcal{D}[v] \quad \text{in } \Omega^e \cup \mathbb{R}^3 \setminus \Omega^e, \quad (31)$$

where \mathcal{S} and \mathcal{D} are the single-layer and double-layer potentials associated with the Helmholtz equation, defined such that

$$\mathcal{S}\lambda(\mathbf{x}) = \int_{\Gamma_\infty} G(\mathbf{x}, \mathbf{y})\lambda(\mathbf{y}) d\mathbf{y}, \quad \mathcal{D}\mu(\mathbf{x}) = \int_{\Gamma_\infty} \frac{\partial G(\mathbf{x}, \mathbf{y})}{\partial n_x} \lambda(\mathbf{y}) d\mathbf{y}, \quad \forall \mathbf{x} \in \Omega^e \cup \mathbb{R}^3 \setminus \Omega^e,$$

where $G(\mathbf{x}, \mathbf{y}) := \frac{\exp(-ik_\infty|\mathbf{x}-\mathbf{y}|)}{4\pi|\mathbf{x}-\mathbf{y}|}$ is a fundamental solution to the classical Helmholtz equation with wavenumber k_∞ . If v is a radiating Helmholtz solution, then [41, Theorem 3.1.2]

$$\begin{bmatrix} \frac{1}{2}I - D & S \\ N & \frac{1}{2}I + D^* \end{bmatrix} \begin{bmatrix} [v]_{\Gamma_\infty} \\ [\nabla v \cdot \mathbf{n}]_{\Gamma_\infty} \end{bmatrix} = - \begin{bmatrix} v^i \\ \nabla v^i \cdot \mathbf{n} \end{bmatrix} \quad \text{on } \Gamma_\infty, \quad (32)$$

where S , D , D^* and N are respectively the single-layer, double-layer, transpose of the double-layer and hypersingular boundary integral operators defined as, $\forall \mathbf{x} \in \Gamma_\infty$,

$$\begin{aligned} S\lambda(\mathbf{x}) &= \int_{\Gamma_\infty} G(\mathbf{x}, \mathbf{y})\lambda(\mathbf{y})d\mathbf{y}, & D\mu(\mathbf{x}) &= \int_{\Gamma_\infty} \frac{\partial G(\mathbf{x}, \mathbf{y})}{\partial n_y} \mu(\mathbf{y})d\mathbf{y}, \\ D^*\lambda(\mathbf{x}) &= \int_{\Gamma_\infty} \frac{\partial G(\mathbf{x}, \mathbf{y})}{\partial n_x} \lambda(\mathbf{y})d\mathbf{y}, & N\mu(\mathbf{x}) &= \oint_{\Gamma_\infty} \frac{\partial^2 G(\mathbf{x}, \mathbf{y})}{\partial n_x \partial n_y} \mu(\mathbf{y})d\mathbf{y}. \end{aligned}$$

Rigorous construction of the operators can be found in [36][Operators on the Boundary, p.217–219]. Consider the function u such that $u|_{\widetilde{\Omega^e}} := f^e$ and $u|_{\widetilde{\Omega^i}} := 0$, where f^e solves (15), so that u is a radiating Helmholtz solution in the transformed coordinates and on the transformed geometry.

Remark 3.6. We chose $u|_{\widetilde{\Omega^i}} := 0$ to ensure that $u|_{\widetilde{\Omega^i}}$ solves the Helmholtz equation in Ω^i , which is clearly the case, and to ensure that u is a radiating Helmholtz solution, to apply (32). We could have chosen any solution to the Helmholtz equation in Ω^i for $u|_{\widetilde{\Omega^i}}$, but in this case, the relation (32) would have involve jumps of traces of some function not related to the problem. Our choice is motivated by the fact that, with $u|_{\widetilde{\Omega^e}} := f^e$ and $u|_{\widetilde{\Omega^i}} := 0$, $[u]_{\widetilde{\Gamma_\infty}} = f^e|_{\widetilde{\Gamma_\infty}}$ and $[\nabla u \cdot \mathbf{n}]_{\widetilde{\Gamma_\infty}} = \widetilde{\nabla} f^e \cdot \widetilde{\mathbf{n}}|_{\widetilde{\Gamma_\infty}}$, so that the relation (32) only involves the total transformed acoustic potential on $\widetilde{\Gamma_\infty}$, which will provide a simple coupling with (30).

Consider the transmission conditions (4), lines 3 and 4. Applying the Prandtl–Glauert transformation (using the first line of (17) and (18)) and making use of (23), there holds

$$\begin{cases} [f]_{\widetilde{\Gamma_\infty}} = 0, \\ [\widetilde{\nabla} f \cdot \widetilde{\mathbf{n}}]_{\widetilde{\Gamma_\infty}} = 0, \end{cases} \quad (33)$$

which we can write

$$\begin{aligned} f^i &= f^e = f, & \text{on } \widetilde{\Gamma}_\infty, \\ \widetilde{\nabla} f^i \cdot \widetilde{\mathbf{n}} &= \widetilde{\nabla} f^e \cdot \widetilde{\mathbf{n}} = \widetilde{\nabla} f \cdot \widetilde{\mathbf{n}}, & \text{on } \widetilde{\Gamma}_\infty. \end{aligned} \quad (34)$$

Using (32) with $v = u$ yields

$$\begin{bmatrix} \frac{1}{2}I - \widetilde{D} & \widetilde{S} \\ \widetilde{N} & \frac{1}{2}I + \widetilde{D}^* \end{bmatrix} \begin{bmatrix} f \\ \widetilde{\nabla} f \cdot \widetilde{\mathbf{n}} \end{bmatrix} = \begin{bmatrix} 0 \\ 0 \end{bmatrix}, \quad \text{on } \widetilde{\Gamma}_\infty, \quad (35)$$

where \widetilde{S} , \widetilde{D} , \widetilde{D}^* and \widetilde{N} are respectively the single-layer, double-layer, transpose of the double-layer and hypersingular boundary integral operators for the Helmholtz equation $\nabla + (\tilde{k}_\infty)^2$ obtained in the Prandtl–Glauert transformed space:

$$\begin{aligned} \widetilde{S}\lambda(\tilde{\mathbf{x}}) &= \int_{\widetilde{\Gamma}_\infty} \hat{G}(\tilde{\mathbf{x}}, \tilde{\mathbf{y}}) \lambda(\tilde{\mathbf{y}}) d\tilde{\mathbf{y}}, & \widetilde{D}\mu(\tilde{\mathbf{x}}) &= \int_{\widetilde{\Gamma}_\infty} \frac{\partial \hat{G}(\tilde{\mathbf{x}}, \tilde{\mathbf{y}})}{\partial \tilde{n}_y} \mu(\tilde{\mathbf{y}}) d\tilde{\mathbf{y}}, \\ \widetilde{D}^*\lambda(\tilde{\mathbf{x}}) &= \int_{\widetilde{\Gamma}_\infty} \frac{\partial \hat{G}(\tilde{\mathbf{x}}, \tilde{\mathbf{y}})}{\partial \tilde{n}_x} \lambda(\tilde{\mathbf{y}}) d\tilde{\mathbf{y}}, & \widetilde{N}\mu(\tilde{\mathbf{x}}) &= \oint_{\widetilde{\Gamma}_\infty} \frac{\partial^2 \hat{G}(\tilde{\mathbf{x}}, \tilde{\mathbf{y}})}{\partial \tilde{n}_x \partial \tilde{n}_y} \mu(\tilde{\mathbf{y}}) d\tilde{\mathbf{y}}, \end{aligned}$$

where $\hat{G}(\mathbf{x}, \mathbf{y}) := \frac{\exp(-ik_\infty|\mathbf{x}-\mathbf{y}|)}{4\pi|\mathbf{x}-\mathbf{y}|}$ is the fundamental solution to the classical Helmholtz equation with modified wavenumber k_∞ .

Using the first line of (35), there holds

$$\widetilde{\nabla} f \cdot \widetilde{\mathbf{n}} = \widetilde{S}^{-1} \left(\widetilde{D} - \frac{1}{2}I \right) (f). \quad (36)$$

Then, we subtract $\widetilde{\nabla} f \cdot \widetilde{\mathbf{n}}$ from the second line of (35) and inverse the signs to obtain

$$\widetilde{\nabla} f \cdot \widetilde{\mathbf{n}} = -\widetilde{N}(f) + \left(\frac{1}{2}I - \widetilde{D}^* \right) \left(\widetilde{\nabla} f \cdot \widetilde{\mathbf{n}} \right). \quad (37)$$

Injecting (36) into the right-hand side of (37), an expression of the $\widetilde{\Lambda}_\infty$ map can be obtained in the following form:

$$\widetilde{\nabla} f \cdot \widetilde{\mathbf{n}} = \widetilde{\Lambda}_\infty(f) := -\widetilde{N}(f) + \left(\frac{1}{2}I - \widetilde{D}^* \right) \widetilde{S}^{-1} \left(\widetilde{D} - \frac{1}{2}I \right) (f). \quad (38)$$

Notice that other $\widetilde{\Lambda}_\infty$ maps can be readily obtained from (35). Our choice leads to a symmetric linear system (see the matrix (54)), for which computation optimizations can be used.

Remark 3.7. *Even though it is possible to write integral equations for the uniformly convected Helmholtz equation (see [7]), the Prandtl–Glauert transformation allows us to write integral equation that only involves the Green kernel associated to the Helmholtz equation. Hence, we can profit from our validated code ACTIPOLE developed by our team [21, 22].*

3.5 Computation of the coupling integral term I_M (11)

The engine is modeled by a semi-infinite waveguide with the classical hypothesis that the flow is uniform. To simplify the presentation, the waveguide is also supposed to be oriented along the local axis \mathbf{e}_z so that Γ_M is orthogonal to \mathbf{e}_z (see Figure 2). More precisely, we suppose here that Γ_M is included in the plane $z = 0$. The flow is defined by \mathbf{M}_M and is then parallel to \mathbf{e}_z . A more general formulation is presented in appendix B.

In Ω_M , the acoustic potential is decomposed into an incident and a diffracted potential: $\varphi := \varphi^{\text{inc}} + \varphi^{\text{diff}}$, both solution to the following convected Helmholtz equation:

$$\Delta \varphi^{\text{inc,diff}} + k_M^2 \varphi^{\text{inc,diff}} + 2ik_M \mathbf{M}_M \cdot \nabla \varphi^{\text{inc,diff}} - \mathbf{M}_M \cdot \nabla \left(\mathbf{M}_M \cdot \nabla \varphi^{\text{inc,diff}} \right) = 0 \quad \text{in } \Omega_M. \quad (39)$$

The incident potential is known, whereas the diffracted potential is unknown. Under these assumptions, the following decomposition holds [38, 13]:

$$\begin{aligned}\varphi^{\text{inc}}(x, y, z) &= \sum_{(\iota)} \alpha_{\iota} v_{\iota}(x, y) \exp(ik_{\iota}^{+}z) \quad \text{in } \Omega_M, \\ \varphi^{\text{diff}}(x, y, z) &= \sum_{(\iota)} \beta_{\iota} v_{\iota}(x, y) \exp(ik_{\iota}^{-}z) \quad \text{in } \Omega_M,\end{aligned}\tag{40}$$

with ι a discrete index and where the incident modal coefficients $\alpha_{\iota} := \int_{\Gamma_M} \varphi^{\text{inc}} \overline{v_{\iota}}$ are supposed known (input of the problem) while the diffracted modal coefficients $\beta_{\iota} := \int_{\Gamma_M} \varphi^{\text{diff}} \overline{v_{\iota}}$ are some unknowns of the problem. The basis functions v_{ι} constitute a modal basis function chosen to be orthonormal.

For instance for a cylindrical duct of radius R , ι corresponds to a couple of indices $(m, n) \in (\mathbb{Z} \times \mathbb{N}^*)$ and the functions v_{ι} are defined in polar coordinates by [38, 13]

$$v_{\iota}(r, \theta) = v_{m,n}(r, \theta) := V_{m,n} J_m\left(\frac{r_{m,n}}{R}r\right) \exp(im\theta),\tag{41}$$

with $r_{m,n}$ the n -th zero of the derivative of m -th Bessel function of the first kind J_m , $V_{m,n}$ the normalization factor such that $\int_{\Gamma_M} v_{m,n}^2 = 1$, and

$$k_{\iota}^{\pm} = k_{mn}^{\pm} = \frac{-k_M M_M \pm \sqrt{k_M^2 - (1 - M_M^2) \left(\frac{r_{m,n}}{R}\right)^2}}{1 - M_M^2} \quad \text{for propagating modes } (k_{mn}^{\pm} \in \mathbb{R}),\tag{42}$$

$$k_{\iota}^{\pm} = k_{mn}^{\pm} = \frac{-k_M M_M \pm i \sqrt{(1 - M_M^2) \left(\frac{r_{m,n}}{R}\right)^2 - k_M^2}}{1 - M_M^2} \quad \text{for evanescent modes } (k_{mn}^{\pm} \in \mathbb{C}),\tag{43}$$

the wavenumber of each mode. For any $(m, n) \in (\mathbb{Z} \times \mathbb{N}^*)$, the corresponding mode is either propagating or evanescent. For any shape of the duct, there exist a finite number of propagating modes and an infinite number of evanescent modes.

Based on this decomposition, the expression of the Dirichlet-to-Neumann operator Λ_M is [10, 33]:

$$(\nabla \varphi - (\mathbf{M}_M \cdot \nabla \varphi) \mathbf{M}_M + ik_M \varphi \mathbf{M}_M) \cdot \mathbf{n} = \Lambda_M(\varphi) := \sum_{(\iota)} (\alpha_{\iota} Y_{\iota}^{+} + \beta_{\iota} Y_{\iota}^{-}) v_{\iota} \quad \text{on } \Gamma_M,\tag{44}$$

where

$$Y_{\iota}^{\pm} := -i [k_{\iota}^{\pm} (1 - M_M^2) + k_M M_M]\tag{45}$$

By definition,

$$\begin{aligned}I_M(\varphi, \varphi^t) &= -\frac{\rho_M}{\rho_{\infty}} \int_{\Gamma_M} \Lambda_M(\varphi) \overline{\varphi^t} \\ &= -\frac{\rho_M}{\rho_{\infty}} \sum_{(\iota)} \alpha_{\iota} Y_{\iota}^{+} \int_{\Gamma_M} v_{\iota} \overline{\varphi^t} - \frac{\rho_M}{\rho_{\infty}} \sum_{(\iota)} \beta_{\iota} Y_{\iota}^{-} \int_{\Gamma_M} v_{\iota} \overline{\varphi^t}.\end{aligned}$$

Notice that since Γ_M is included in the plane $z = 0$ and M_{∞} is directed along \mathbf{e}_z , then $\widetilde{\Gamma}_M = \Gamma_M$, and $\widetilde{v}_{\iota} = v_{\iota}$ on Γ_M , where \widetilde{v}_{ι} is the Prandtl–Glauert transformation of v_{ι} . Hence, $\alpha_{\iota} = \int_{\widetilde{\Gamma}_M} f^{\text{inc}} \overline{\widetilde{v}_{\iota}}$ and $\beta_{\iota} = \int_{\widetilde{\Gamma}_M} f^{\text{diff}} \overline{\widetilde{v}_{\iota}}$, where f^{inc} and f^{diff} are the Prandtl–Glauert transformation of respectively φ^{inc} and φ^{diff} . In view of the coupling in the coordinates and geometry transformed by the Prandtl–Glauert transformation, we can write

$$I_M(\varphi, \varphi^t) = -\frac{\rho_M}{\rho_{\infty}} \sum_{(\iota)} (\alpha_{\iota} Y_{\iota}^{+} + \beta_{\iota} Y_{\iota}^{-}) \int_{\widetilde{\Gamma}_M} \widetilde{v}_{\iota} \overline{f^t}\tag{46}$$

with f^t the Prandtl–Glauert transformation of φ^t . Let us define γ_κ by $f^t = \sum_{(\kappa)} \gamma_\kappa \tilde{v}_\kappa$. Then, using the orthonormality of the modal basis $\int_{\Gamma_M} \tilde{v}_\iota \overline{\tilde{v}_\kappa} = \delta_{\iota,\kappa}$, where $\delta_{\iota,\kappa}$ refers to the Kronecker delta, we obtain

$$I_M(\varphi, \varphi^t) = -\frac{\rho_M}{\rho_\infty} \sum_{(\iota)} (\alpha_\iota Y_\iota^+ + \beta_\iota Y_\iota^-) \overline{\gamma}_\iota. \quad (47)$$

To write a direct coupled problem, it is more practical to consider the coefficients of the decomposition of the total acoustic potential. Consider $\varsigma_\iota := \int_{\Gamma_M} \varphi \overline{v}_\iota = \alpha_\iota + \beta_\iota$, there holds

$$I_M(\varphi, \varphi^t) = -\frac{\rho_M}{\rho_\infty} \sum_{(\iota)} (\alpha_\iota (Y_\iota^+ - Y_\iota^-) + \varsigma_\iota Y_\iota^-) \overline{\gamma}_\iota. \quad (48)$$

3.6 Transformed coupled problem

Let Ω be a Lipschitz domain in \mathbb{R}^3 , and $\Gamma = \partial\Omega$. Define the trace operator γ as $\gamma u = u|_\Gamma$, where u is a smooth function compactly supported on $\overline{\Omega}$. From [36][Theorem 3.37], the trace operator γ is bounded from $H^1(\Omega)$ to $L^2(\Gamma)$, and $H^{\frac{1}{2}}(\Gamma)$ can be defined as the image of $H^1(\Omega)$ by γ . Then, $H^{-\frac{1}{2}}(\Gamma)$ is a realization of the dual space of $H^{\frac{1}{2}}(\Gamma)$ with the norm $\|u\|_{H^{-\frac{1}{2}}(\Gamma)} = \sup_{0 \neq v \in H^{\frac{1}{2}}(\Gamma)} |(u, v)_\Gamma| / \|v\|_{H^{\frac{1}{2}}(\Gamma)}$, where $(u, v)_\Gamma = \int_\Gamma \overline{u} v$, with \overline{u} the complex conjugate of u .

To treat the operator inversion in the definition (38) of $\widetilde{\Lambda}_\infty$, we introduce $\lambda \in H^{-\frac{1}{2}}(\widetilde{\Gamma}_\infty)$ such that

$$\lambda := (\widetilde{S})^{-1} \circ \left(\left(\widetilde{D} - \frac{1}{2}I \right) f \right), \quad (49)$$

so that

$$\begin{cases} \widetilde{\Lambda}_\infty(f) = -\widetilde{N}f + \left(\frac{1}{2}I - \widetilde{D}^* \right) \lambda, \\ \left(\widetilde{D} - \frac{1}{2}I \right) f - \widetilde{S}\lambda = 0. \end{cases} \quad (50)$$

Plugging (50) into (30) and using the expression (48) in (8) leads to the following weak formulation for the coupled problem: find $(f, \lambda) \in H^1(\widetilde{\Omega}^i) \times H^{-\frac{1}{2}}(\widetilde{\Gamma}_\infty)$ such that $\forall (f^t, \lambda^t) \in H^1(\widetilde{\Omega}^i) \times H^{-\frac{1}{2}}(\widetilde{\Gamma}_\infty)$,

$$\begin{cases} \widetilde{a}(f, f^t) + J_\infty \int_{\widetilde{\Gamma}_\infty} \widetilde{N}f \overline{f^t} + J_\infty \int_{\widetilde{\Gamma}_\infty} \left(\widetilde{D}^* - \frac{1}{2}I \right) \lambda \overline{f^t} - \frac{\rho_M}{\rho_\infty} \sum_{(\iota)} \varsigma_\iota Y_\iota^- \overline{\gamma}_\iota \\ = \frac{\rho_M}{\rho_\infty} \sum_{(\iota)} \alpha_\iota (Y_\iota^+ - Y_\iota^-) \overline{\gamma}_\iota, \\ J_\infty \int_{\widetilde{\Gamma}_\infty} \left(\widetilde{D} - \frac{1}{2}I \right) f \overline{\lambda^t} - J_\infty \int_{\widetilde{\Gamma}_\infty} \widetilde{S}\lambda \overline{\lambda^t} = 0. \end{cases} \quad (51)$$

with ς_ι and γ_ι such that $\sum_{(\iota)} |\varsigma_\iota|^2 |Y_\iota^\pm| < \infty$ and $\sum_{(\iota)} |\gamma_\iota|^2 |Y_\iota^\pm| < \infty$ and with $\widetilde{a}(f, f^t) = a(\varphi, \varphi^t)$, where a is defined in (20).

4 Methodologies for the numerical resolutions

The weak formulation (51) has to be solved numerically. To do so, we first introduce an unstructured volumic mesh \mathcal{V}_h of the domain $\widetilde{\Omega}^i$ made of tetrahedrons. The surfacic meshes $\mathcal{S}_{h,M}$ and $\mathcal{S}_{h,\infty}$ are obtained as the boundary faces of \mathcal{V}_h associated to $\widetilde{\Gamma}_M$ and $\widetilde{\Gamma}_\infty$ respectively. We denote \mathcal{V}_h^1 and $\mathcal{S}_{h,M}^1$ the finite element spaces \mathbb{P}^1 on respectively \mathcal{V}_h and $\mathcal{S}_{h,M}$, and $\mathcal{S}_{h,\infty}^0$ the finite element space \mathbb{P}^0 on $\mathcal{S}_{h,\infty}$. To introduce a numerical approximation, we have to consider a finite number of modes. We consider then $M_{\text{tot}}^{\text{inc}}$ incident modes and $M_{\text{tot}}^{\text{diff}}$ diffracted modes, with $M_{\text{tot}}^{\text{diff}} \geq M_{\text{tot}}^{\text{inc}}$.

We obtain the following discrete conforming approximation of (51): Find $(f_h, \lambda_h) \in \mathcal{V}_h^1 \times \mathcal{S}_{h,\infty}^0$ such that $\forall (f_h^t, \lambda_h^t) \in \mathcal{V}_h^1 \times \mathcal{S}_{h,\infty}^0$,

$$\left\{ \begin{array}{l} \tilde{a}(f_h, f_h^t) + J_\infty \int_{\widetilde{\Gamma}_\infty} \tilde{N} f_h \overline{f_h^t} + J_\infty \int_{\widetilde{\Gamma}_\infty} \left(\tilde{D}^* - \frac{1}{2} I \right) \lambda_h \overline{f_h^t} - \frac{\rho_M}{\rho_\infty} \sum_{(\iota)}^{M'_{\text{tot}} \text{diff}} \overline{\varsigma}_\iota Y_\iota^- \overline{\gamma}_\iota \\ = \frac{\rho_M}{\rho_\infty} \sum_{(\iota)}^{M'_{\text{tot}} \text{diff}} \alpha_\iota (Y_\iota^+ - Y_\iota^-) \overline{\gamma}_\iota, \\ J_\infty \int_{\widetilde{\Gamma}_\infty} \left(\tilde{D} - \frac{1}{2} I \right) f_h \overline{\lambda_h^t} - J_\infty \int_{\widetilde{\Gamma}_\infty} \tilde{S} \lambda_h \overline{\lambda_h^t} = 0, \end{array} \right. \quad (52)$$

with ς_ι and γ_ι such that $\sum_{(\iota)} |\varsigma_\iota|^2 |Y_\iota^\pm| < \infty$ and $\sum_{(\iota)} |\gamma_\iota|^2 |Y_\iota^\pm| < \infty$. Notice that since $M'_{\text{tot}} \text{diff} \geq M_{\text{tot}}^{\text{inc}}$, then some α_ι are zero.

Let $(\theta_i)_{1 \leq i \leq p}$ and $(\psi_i)_{1 \leq i \leq q}$ denote finite element bases for \mathcal{V}_h^1 and $\mathcal{S}_{h,\infty}^0$ respectively. The decomposition of $f_h \in \mathcal{V}_h^1$ and $\lambda_h \in \mathcal{S}_{h,\infty}^0$ on these bases are written in the form $f_h = \sum_{i=1}^p f_i \theta_i$ and $\lambda_h = \sum_{i=1}^q \lambda_i \psi_i$. Let

$$u := \left(\begin{array}{l} (f_i)_{1 \leq i \leq p} \\ (\lambda_i)_{1 \leq i \leq q} \end{array} \right), \quad b := \left(\begin{array}{l} \left(\frac{\rho_M}{\rho_\infty} \sum_{(\iota)}^{M'_{\text{tot}} \text{diff}} \alpha_\iota (Y_\iota^+ - Y_\iota^-) \int_{\Gamma_M} \tilde{v}_\iota \overline{\theta}_i \right)_{1 \leq i \leq p} \\ (0)_{1 \leq i \leq q} \end{array} \right), \quad (53)$$

and

$$A := \left(\begin{array}{c|c} C_{ij} & J_\infty \int_{\widetilde{\Gamma}_\infty} \left(\tilde{D}^* - \frac{1}{2} I \right) \psi_j \overline{\theta}_i \\ \hline J_\infty \int_{\widetilde{\Gamma}_\infty} \left(\tilde{D} - \frac{1}{2} I \right) \theta_j \overline{\psi}_i & -J_\infty \int_{\widetilde{\Gamma}_\infty} \tilde{S} \psi_j \overline{\psi}_i \end{array} \right), \quad (54)$$

with

$$C_{ij} := \tilde{a}(\theta_j, \theta_i) + J_\infty \int_{\widetilde{\Gamma}_\infty} \tilde{N} \theta_j \overline{\theta}_i - \frac{\rho_M}{\rho_\infty} \sum_{(\iota)}^{M'_{\text{tot}} \text{diff}} Y_\iota^- \int_{\Gamma_M} \tilde{v}_\iota \overline{\theta}_i \int_{\Gamma_M} \theta_j \overline{\tilde{v}_\iota}. \quad (55)$$

The linear system resulting from (51) is

$$Au = b. \quad (56)$$

The matrix A contains both dense and sparse blocks. By reordering the unknowns in order to separate the unknowns related to $\widetilde{\Omega}^i$ and to $\widetilde{\Gamma}_\infty$ (indexed respectively by V and Γ in the following), the linear system can be written

$$\begin{pmatrix} A_{VV} & A_{V\Gamma} \\ A_{\Gamma V} & A_{\Gamma\Gamma} \end{pmatrix} \begin{pmatrix} u_V \\ u_\Gamma \end{pmatrix} = \begin{pmatrix} b_V \\ b_\Gamma \end{pmatrix} \quad (57)$$

with A_{VV} , $A_{V\Gamma}$ and $A_{\Gamma V}$ being sparse matrices and $A_{\Gamma\Gamma}$ a dense matrix.

To solve (57), a block Gaussian elimination, known as the Schur complement [52], is first carried out on the sparse matrices to eliminate the unknowns of the volume domain. The remaining system is then

$$(A_{\Gamma\Gamma} - A_{\Gamma V} A_{VV}^{-1} A_{V\Gamma}) u_\Gamma = b_\Gamma - A_{\Gamma V} A_{VV}^{-1} b_V \quad (58)$$

This linear system can then be solved either with a direct classical LU solver or an iterative solver. Moreover in the case of the iterative solver, the fast multipole method (FMM) [44, 48, 29] can be used to take into account the dense matrix $A_{\Gamma\Gamma}$ relative to the BEM formulation. The conditioning of the remaining system is driven by the BEM matrix. The classical SPAI preconditioner for BEM

formulation [15] of matrix $A_{\Gamma\Gamma}$ is then used to improve the converge of the iterative solver for equation (58).

These resolution strategies are implemented in the ACTIPOLE software and make use of the MUMPS solver [3, 4] for the sparse matrix elimination and of an in-house solver with out-core and MPI functionalities for the remaining system.

5 Numerical results

Even if the test cases are axisymmetric, all the following computations are full-3D computations. They have been run on a machine with 2x6 intel Xeon “Westmere” processors running at 3.06GHz with 72GB RAM per node and infiniband QDR.

5.1 Zero flow

The first test case is designed to check the validity of the modeling for a non-uniform medium without flow and of the FEM-BEM coupling. It consists of a sphere of radius 1 m centered at the origin with different fluid properties: $\rho_0 = \rho_\infty$, $c_0 = 2c_\infty$ inside the sphere and $\rho_\infty = 1.2 \text{ kg.m}^{-3}$, $c_\infty = 340 \text{ m.s}^{-1}$ outside the sphere. The acoustic potential source is a monopole located outside the sphere at $(0, 0, 2.5)$. The observable is located outside the sphere at $(0, 1.7, 0)$ and the frequency range of interest is 11 to 500 Hz.

The reference result is obtained by a Mie series and the comparison of the scattered pressure with the FEM-BEM solution is visible on Figure 4. The volumic domain used for the FEM-BEM computation is a sphere of radius 1.07 m to ensure the continuity of the speed of sound at Γ_∞ . The mesh has an average edge length of 85 mm ($\lambda/8$ for 500 Hz, the highest frequency) and contains 19,494 dofs (80,616 tetrahedrons and 4,672 triangles on Γ_∞). The relative error on the module of the total pressure is between 7×10^{-4} (at 100 Hz) and 3×10^{-2} (at 500 Hz).

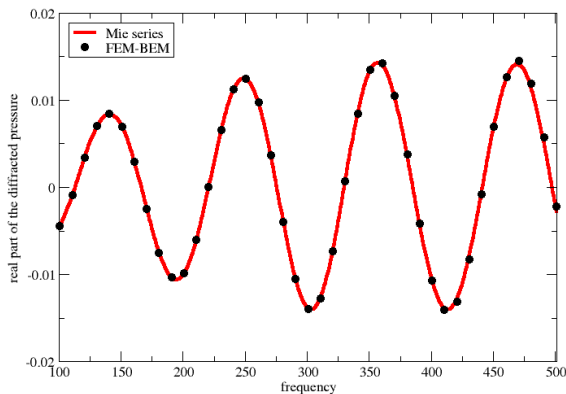


Figure 4: Zero flow: Real part of the scattered pressure at the sensor in function of the frequency (validation of the FEM-BEM on the sphere test case).

5.2 Modal test case without flow

Consider a modal cylindrical duct of length $L = 1$ m and radius $R = 0.25$ m without flow (Figure 5). The frequency of the source is 2,040 Hz. Three kinds of computation have been performed with ACTIPOLE: classical BEM formulation, full FEM formulation, coupled FEM-BEM formulation in the same domain of computation. The iterative solver has been chosen with a tolerance on the residual of 10^{-8} . Comparisons have been carried out on the transmission coefficients between Γ_{M_1} and Γ_{M_2} of the mode $m = 0$, $n = 1$ (Table 1) and their theoretical values.

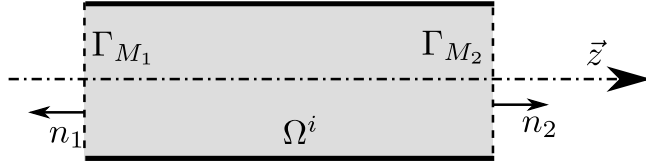


Figure 5: Geometry of the modal test case.

Mean edge	20 mm ($\lambda/8$)	16 mm ($\lambda/10$)	11m m ($\lambda/15$)	8 mm ($\lambda/20$)
BEM only, FMM	9.6×10^{-3}	3.1×10^{-3}	1.2×10^{-3}	2.4×10^{-4}
FEM-BEM, FMM	0.28	0.19	0.08	4.6×10^{-2}
FEM only, iterative	0.55	0.36	0.16	0.09

Table 1: Relative error on the transmission coefficient for the mode (0,1).

As expected, due to finite element dispersion, the mesh must be finer in the FEM part than in the BEM part to have an acceptable error. Moreover the error obtained here by the FEM on the transmission coefficient has a linear dependency on the length of the FEM domain and a square dependency on the size of the elements.

5.3 Modal test case with a uniform flow

Consider the previous modal test case with a uniform flow in the direction of the duct, with a Mach number of 0.6. The frequency of the source is chosen such that the mean number of elements per wavelength after the Prandtl–Glauert transformation remains the same as the previous configuration meshes (without flow) of Section 5.2. We recall that the Prandtl–Glauert transformation consists in a space dilatation (12) and a frequency change (15). The frequency is then 1305 Hz.

The results on the transmission coefficient for the modes (0, 1) are compared with their theoretical values. The coefficients for both a propagation with the flow (emission on Γ_{M_1}) and against the flow (emission on Γ_{M_2}) are considered. A computation has also been added to the previous tested configurations. It consists in the case of the full FEM model without any flow in the exterior external domain ($M_\infty = 0$). The results are presented on Table 2.

Propagation with the flow (emission on modal surface Γ_{M_1} , reception on Γ_{M_2})

Mean edge		20 mm ($\lambda'/8$)	16 mm ($\lambda'/10$)	11 mm ($\lambda'/15$)	8 mm ($\lambda'/20$)
BEM only, FMM	$M_M = M_\infty = 0.6$	1.2×10^{-2}	4.2×10^{-3}	1.6×10^{-3}	5.5×10^{-4}
FEM-BEM, FMM	$M_M = M_\infty = 0.6$	0.31	0.21	0.09	0.05
FEM only, iterative	$M_M = M_\infty = 0.6$	0.61	0.40	0.17	0.10
FEM only, iterative	$M_M = 0.6, M_\infty = 0$	0.0163	0.010	0.0045	2.5×10^{-3}

Propagation against the flow (emission on modal surface Γ_{M_2} , reception on Γ_{M_1})

Mean edge		20 mm ($\lambda'/8$)	16 mm ($\lambda'/10$)	11 mm ($\lambda'/15$)	8 mm ($\lambda'/20$)
BEM only, FMM	$M_M = M_\infty = 0.6$	1.2×10^{-2}	4.2×10^{-3}	1.6×10^{-3}	5.6×10^{-4}
FEM-BEM, FMM	$M_M = M_\infty = 0.6$	0.31	0.21	0.09	0.05
FEM only, iterative	$M_M = M_\infty = 0.6$	0.61	0.40	0.17	0.10
FEM only, iterative	$M_M = 0.6, M_\infty = 0$	2.00	1.60	0.48	0.02

Table 2: Relative error on the transmission coefficient for the mode (0, 1), $M_M = 0.6$

We can see in the first three lines of each array of Table 2 that the errors are very similar to the previous case without flow. The small differences are due to the fact that even if the size of mesh is adapted to the Prandtl–Glauert transformation, the mesh is slightly distorted by the transformation

(the dilatation factor in the direction of the flow is 1.25). Moreover, with the Prandtl–Glauert transformation, the error is identical whether the mode propagates with or against the flow. As expected, if the flow outside the duct is zero (fourth line of the arrays of Table 2), the accuracy is different whether the wave propagates with or against the flow inside the duct (with respectively large or small equivalent wavelengths). Then if the potential flow is close to the flow at infinity, by using the Prandtl–Glauert transformation, a better control on the mesh size and the accuracy can be obtained.

5.4 Toward engineering applications

5.4.1 Rigid sphere into a potential flow

The next test case is the case of a rigid sphere of radius $R_s = 0.6$ m in a flow. The acoustic source consists of a potential monopole at a frequency of 1133 Hz and a distance of 1.2 m from the surface of the sphere, defined by

$$\varphi^{\text{inc}} = \frac{e^{ikr}}{4\pi r}. \quad (59)$$

We consider two configurations:

1. a uniform flow defined by $\mathbf{M}_\infty = 0.4\mathbf{e}_z$. There is no interior domain Ω^i , and the boundary conditions at Γ are clearly violated,
2. an incompressible analytic potential flow around the sphere (Equation (60) for $r < R_\infty$) combined with a uniform flow far from the sphere ($\mathbf{M}_\infty = 0.4\mathbf{e}_z$ for $r \geq R_\infty$) with a supposed continuity of the flow at the interface. For that we choose $R_\infty = 2R_s = 1.2$ m (Figure 6).

In spherical coordinates, the potential flow in Ω^i in spherical coordinates is such that

$$\mathbf{M}_0(r, \theta, \phi) = M_\infty \cos(\theta) \left[1 - \left(\frac{R_s}{r} \right)^3 \right] \mathbf{e}_r - M_\infty \sin(\theta) \left[1 + \frac{1}{2} \left(\frac{R_s}{r} \right)^3 \right] \mathbf{e}_\theta. \quad (60)$$

The flow is then tangent to Γ , but the continuity condition of the flow through Γ_∞ is not strictly obtained for a finite value of R_∞ .

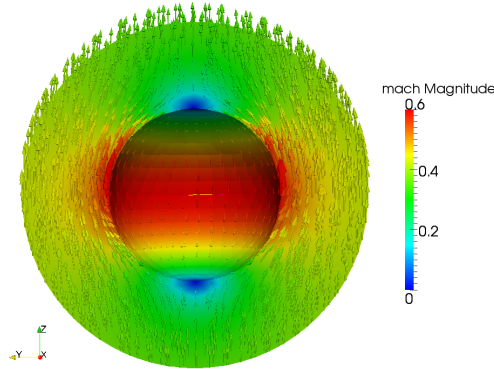


Figure 6: Analytic flow computed around the sphere.

A mesh with an average edge length of 25 mm is used. That represents 6.7×10^5 degrees of freedom in the volume and 10^5 on the surface. The computation took 7 h on 60 processors for the direct solver and 2 h on 24 processors and 568 iterations for the FMM solver for an achieved residual of 10^{-6} .

Figure 7 illustrates that the presence of the potential flow around the sphere has modified the acoustic potential map. Local acoustic velocity and pressure magnitude have increased, as well as its magnitude in the shadow zone. This is also visible on Figure 8, that shows some radiation patterns for the total pressure on a circle of radius 10 m for 3 positions of the emitter ($(0., 0., 1.8)$, $(0., 0., -1.8)$ and $(-1.8, 0., 0)$ respectively). Figure 7 shows that first the radiation pattern is modified by the hypothesis on the flow, and second that this modification is different whether the acoustic waves propagate with or against the flow, with respectively lower and higher level of pressure for the potential model in the shadow region.

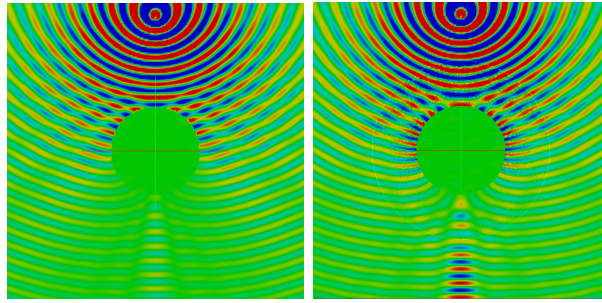


Figure 7: Rigid sphere: real part of the total acoustic pressure for an emitter located at $(0., 0., 1.8)$ (*left*: uniform flow BEM, *right*: potential flow FEM-BEM).

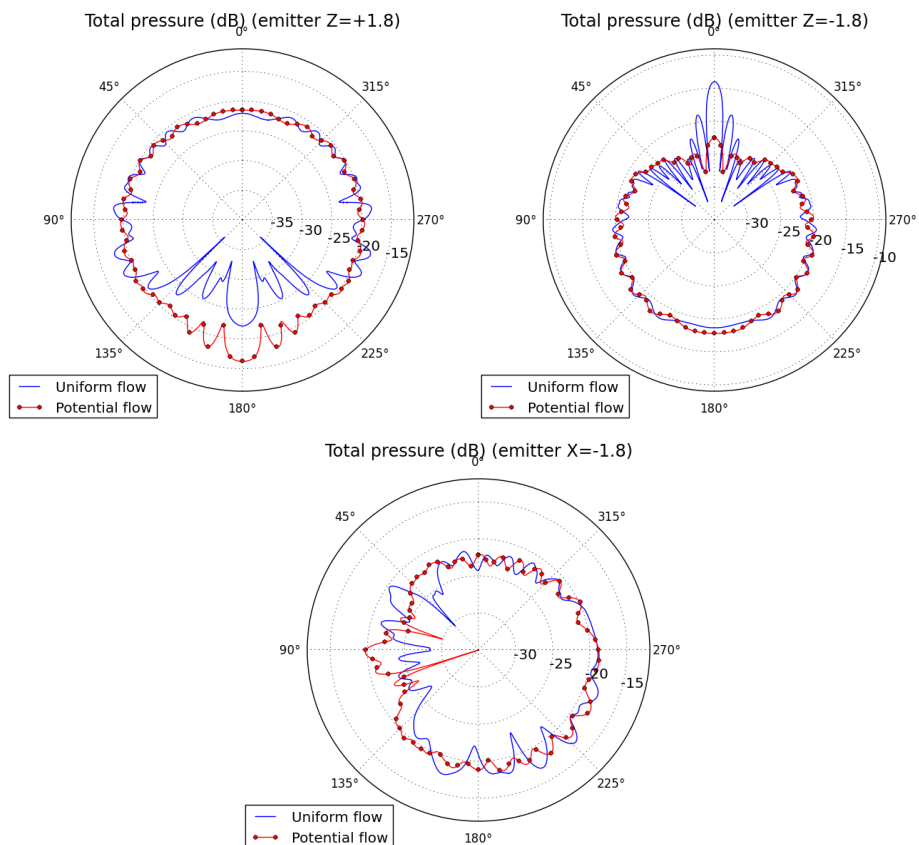


Figure 8: Rigid sphere: acoustic total pressure in dB radiated on a circle at $r = 10$ m for different positions of the emitter

5.4.2 Simplified engine

The next test case is more realistic. It consists of a simplified engine with modal surfaces orthogonal to \mathbf{e}_z to model the upstream and downstream fans (see Figure 9). The far field flow is defined by $\mathbf{M}_\infty = -0.3\mathbf{e}_z$. Three different configurations are considered: a uniform flow defined by \mathbf{M}_∞ and potential flows computed such that the Mach number at the upstream modal surface Γ_M is 0.3 and 0.42.

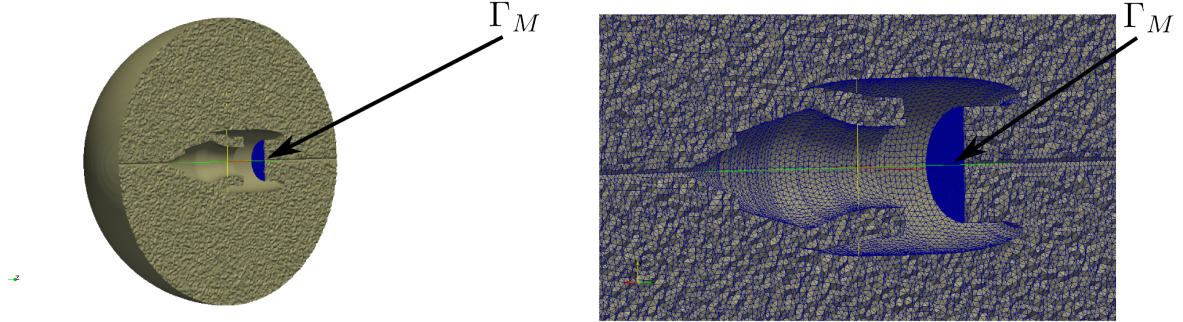


Figure 9: Cut of the mesh of the simplified engine.

First, the potential flow is computed using an in-house software based on a fixed-point algorithm [42, 27]. The potential flow obtained when $M_M = 0.42$ at the upstream modal surface is plotted on Figure 10.

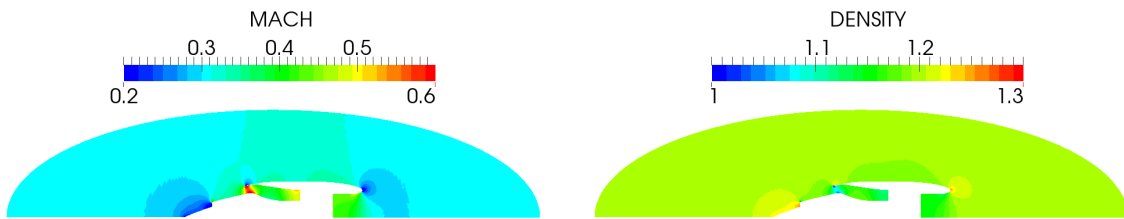


Figure 10: Simplified engine: computed potential flow such that $M_M = 0.42$ and $M_\infty = 0.3$ (left: Mach number, right: density).

We now consider the upstream fan modal source model at the frequency of 200 Hz. The mean size of the mesh elements is 83 mm. The model contains 1.2×10^6 dofs and 11.8×10^6 tetrahedrons. At this frequency and for this flow, there are three to four propagating modes. To be compared, the intensity on each mode is set to 100 dB, following Morfey's convention [37].

The pressure obtained in the vicinity of the modal surface is shown on Figures 11 and 12. For each mode, the top part of the Figure is the pressure obtained with the uniform flow model and the bottom part of the Figure the pressure obtained with the potential model with a Mach number at the modal surface of 0.3 or 0.42. Small variations are observed with the $M_M = 0.3$ condition. The differences are higher when the flow at the modal surface is higher.

Figure 13 shows the pressure in dB obtained on a circle at a distance of 20 m from the center of the modal surface, for different values of M_M . Significant changes in the amplitude are obtained for the different modes by taking into account the potential flow. For instance for the mode (1, 1) and for the same flow at the modal surface, the amplitude predicted for the potential flow is approximately 1 dB lower in the axis direction than the amplitude predicted by the uniform flow model. By increasing the flow through the upstream modal surface, the difference with the uniform flow model is higher and observed for all the radiation directions.

Figure 14 illustrates the influence of the relative residual of the iterative solver on the diffracted pressure field. Results for relative residuals of 10^{-3} and 10^{-6} , and with or without a Schur complement on the volume part of the matrix are presented. From these results, it appears that a convergence with a tolerance of 10^{-3} is not sufficient for a solution without a Schur complement on the volume

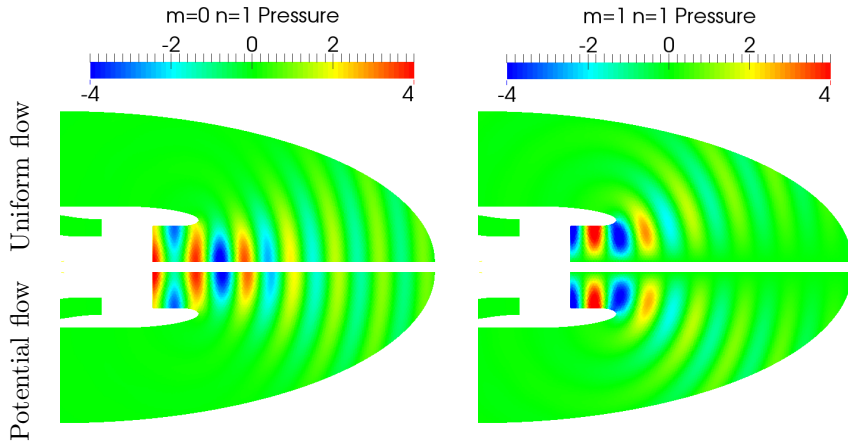


Figure 11: Simplified engine: comparison of the pressure for the uniform model and the potential model with $M_\infty = M_M = 0.3$.

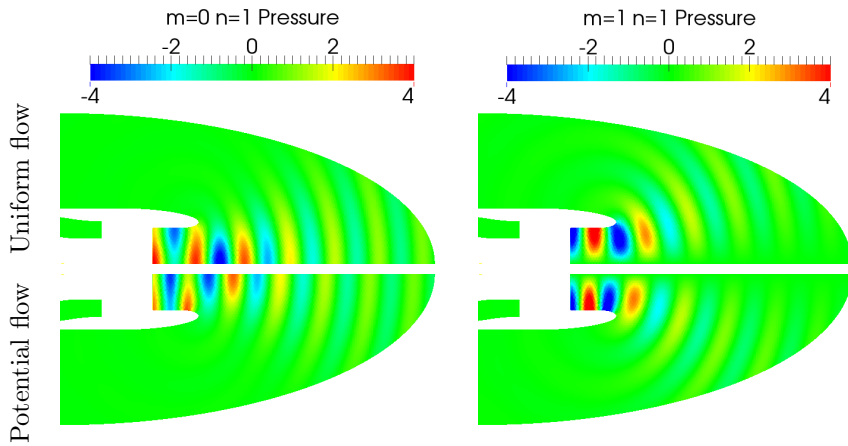


Figure 12: Simplified engine: comparison of the pressure for the uniform model ($M_\infty = M_M = 0.3$) and the potential model ($M_\infty = 0.3$ and $M_M = 0.42$).

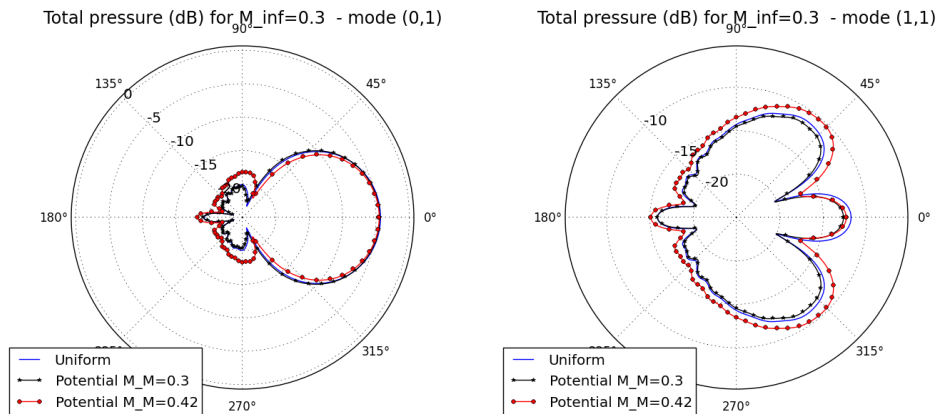


Figure 13: Simplified engine: pressure in dB on a circle at $r = 20$ m for $M_\infty = 0.3$ and some values of M_M (mesh size 75mm).

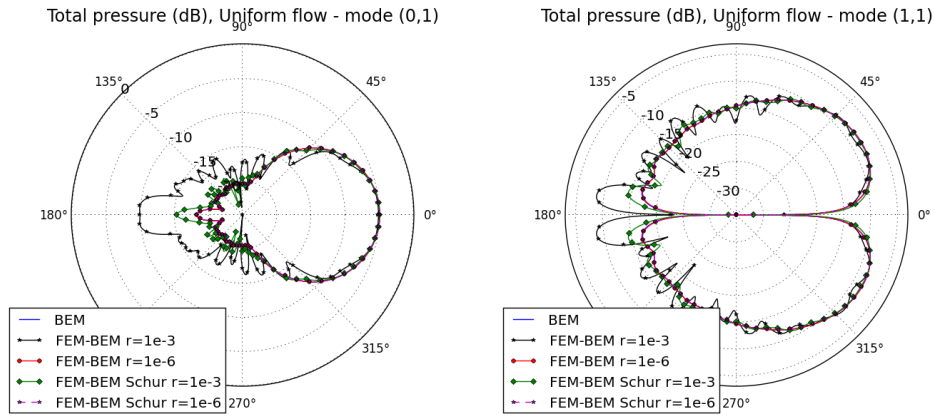


Figure 14: Simplified engine: influence of the convergence criteria and on the pressure in dB on a circle at $r = 20$ m for a uniform flow defined by $M_M = M_\infty = 0.1$.

part of the matrix.

In that case, for a mesh containing 4.7×10^6 dofs and 25.8×10^6 tetrahedrons, the computation took 1.5 h on 160 processors and 231 iterations for the FMM solver without using the Schur complement and 6.5 h on 120 processors and 204 iterations with for an achieved residual of 10^{-6} .

5.4.3 Non-potential realistic flow

This last test case has been done in order to test the method against measurements and evaluate its capabilities in non-potential flow conditions. This test case has been defined and measured in the framework of EU-project TURNEX (Turbomachinery Noise Radiation through the Engine Exhaust) [24, 25]. Different configurations at a 1/10 scale mock-up placed in a semi-anechoic room have been tested. However, only two are used as reference in this test case: the isolated exhaust (nacelle alone), and the installed exhaust (nacelle coupled to a plane swept wing). All the configuration is rigid. The configurations are based on static approach conditions: a realistic flow is generated in the primary and secondary ducts and the external medium is at rest. A realistic jet mixing layer is thus created. The measurements means are for instance presented in [39].

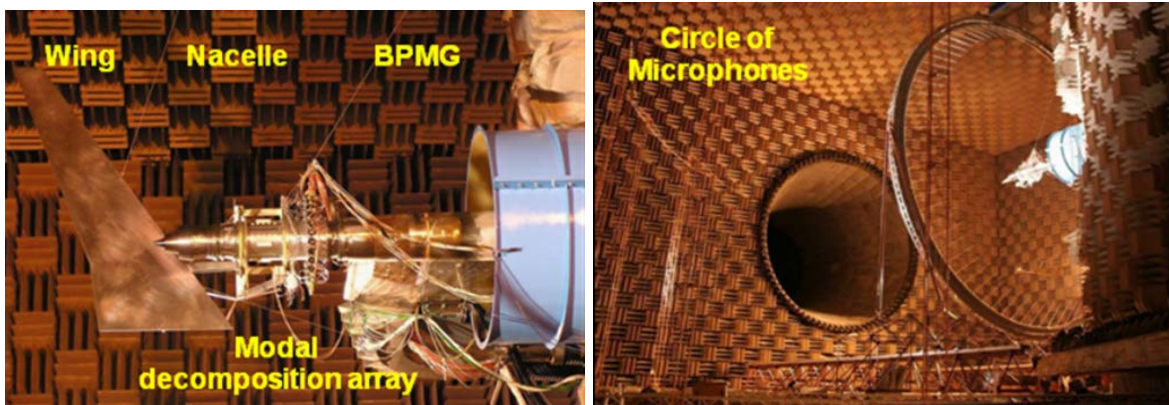


Figure 15: Configuration measurement of TURNEX test case

The acoustic fan source is a modal broadband source installed in the secondary duct, classically modeled by a summation of uncorrelated duct cut-on modes. The acoustic pressure is measured on a circle of microphones which can move along the exhaust axis direction. The results are extrapolated on a sphere of radius 4.8 meters centered on the exhaust outlet. The measurements values are averaged values on third-octave range.

The quantity of interest is the installation effects, that is

$$\text{IFX} = \text{RMS}_{\text{Installed}} - \text{RMS}_{\text{Isolated}}.$$

where RMS is the broadband noise obtained by equipartition of the energy on the azimuthal modes

$$\text{RMS}_{\text{dB}}(\theta) = 10 \log_{10} \left(\sum_m \frac{1}{N_m} \sum_{n=1}^{N_m} P_{mn}(\theta)^2 \right) - 10 \log_{10} (P_{\text{ref}}^2) \quad (61)$$

with P_{ref} the reference pressure ($2 \cdot 10^{-5} \text{Pa}$), N_m the number of radial modes for azimuthal mode m and P_{mn} the radiated pressure of the mode m, n .

Two models of flow are used in the simulation: on one side a flow obtained with a finite volume CFD code that solves Navier-Stokes equations and is interpolated on the acoustic mesh and on the other side a piecewise flow created from an idealized sheared layer. Figure 16 presents the axial velocity field in a cross-section. The piecewise flow has been smoothed in order to match the uniform flow conditions in the external domain.

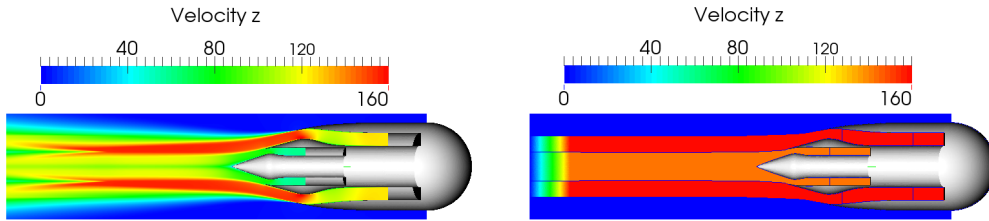


Figure 16: Axial velocity field (CFD and piecewise models)

Results obtained for 5kHz configuration are presented here. Figure 17 illustrates for the isolated and installed configurations the acoustic wave propagation, reflection on the wing and jet blockage. Figure 18 shows installation effects on the sphere of observable and in particular the wing shielding effects (the pattern is no more symmetric due to the wing) the shielding effect due to the mixing layer (also visible on Figure 17). This confirms the good behavior of both code and FE model. Figure 19 shows on the 3 directivity arcs (flyover 0° , sideline $+54^\circ$ and -54°) the results for our method and comparison with measurements data and results obtained with ACTRAN/DGM solver and presented in [39] (Linearized Euler Equation model). The global behaviour is similar between the numerical methods and the measurements. However some discrepancies persist. As detailed in [39], there is a suspicion of a difference of 1dB on the source amplitude between the isolated and installed configuration (for instance, the installed configuration is less noisy than the isolated configuration on the flyover arc). Some deficient microphones are also suspected as visible on Figure 18 where for some arcs near the sideline positions the measured values are very different from the values on the other angles.

However, the method shows a global good agreement with both measurements and the other numerical method despite the potential flow model assumption. Moreover, the results obtained with the approximated piecewise flow model are comparable to the interpolated CFD model. Then, the precise knowledge of the aerodynamic flow field for this model does not seem to be very important.

Further comparisons are running on another configuration with measurements with a higher accuracy.

Different meshing lengths have been used for these computations (5mm and 3mm of averaging length for the edges). The mesh characteristics and computation times are presented in Table 3.

average meshing	3D Mesh				Computation	
	triangles nb	tetras nb	surf. dof nb	vol dof nb	CPU time	Nb. iter.
5mm	145k	5.2M	223k	853k	1h on 120 procs	38
3mm	400k	23.2M	614k	3.85M	14h on 240 procs	26

Table 3: Mesh and computation times for TURNEX computation

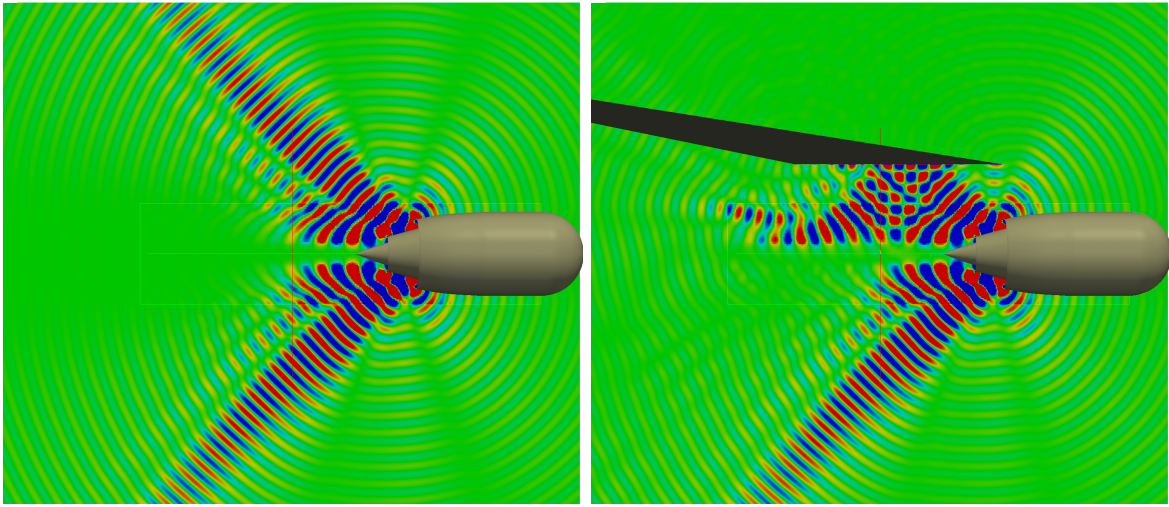


Figure 17: Propagation of mode (2,1) without/with installation effects (acoustic pressure)

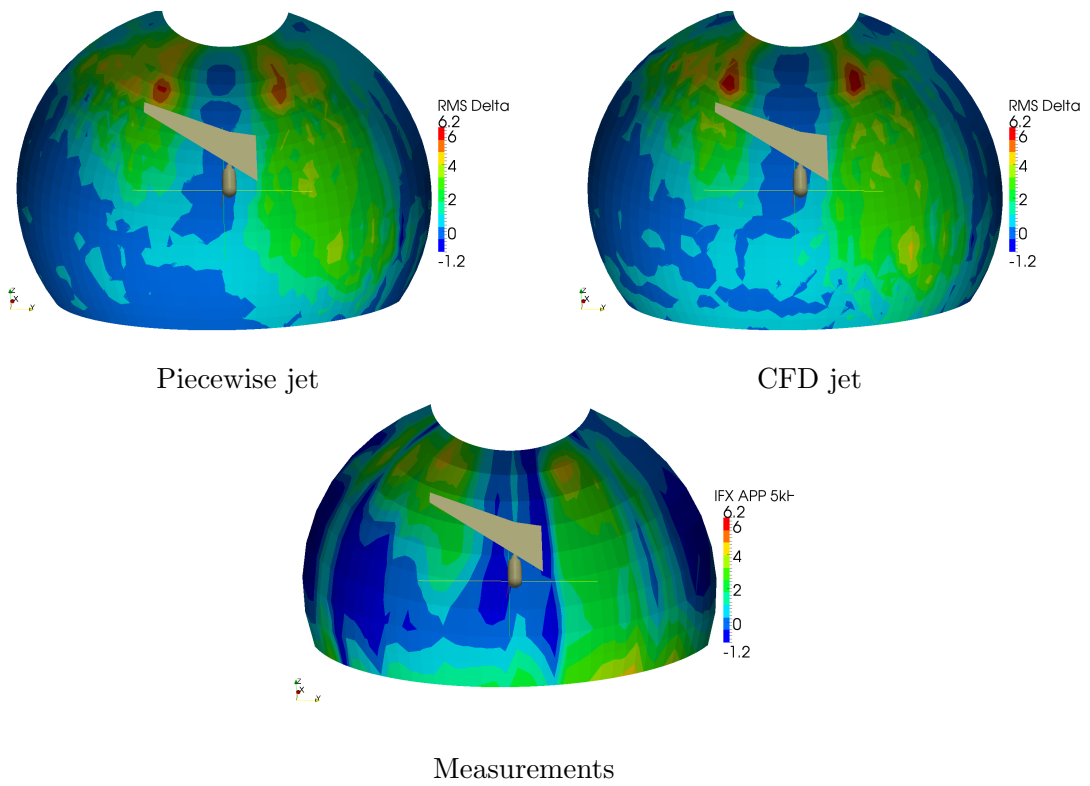


Figure 18: Installation effect IFX on a sphere at $r = 4.8\text{m}$

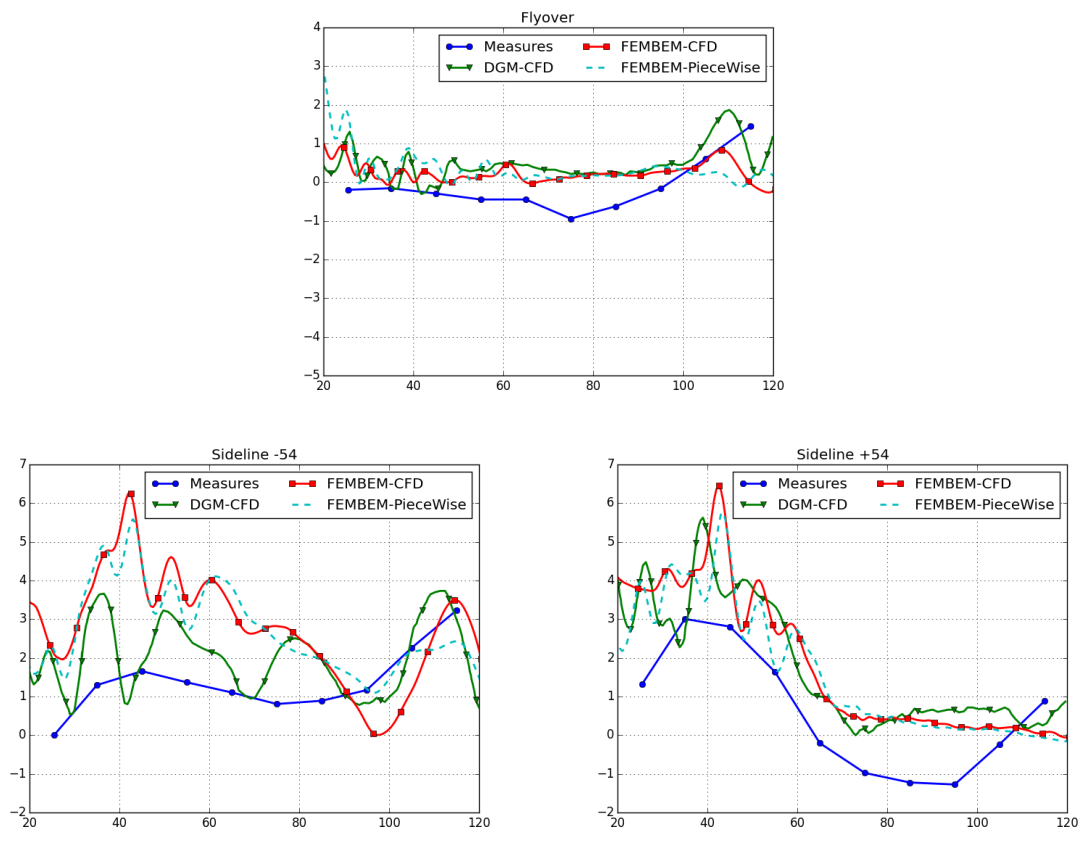


Figure 19: Comparison of the installation effects on flyover and sideline arcs between measurements, ACTRAN/DGM and our method

6 Conclusion

In this work, we derived a direct coupling method to compute the acoustic propagation of the noise generated by a turboreactor in a flow that is potential in a bounded domain containing the object, and uniform elsewhere. This approach, that decouples the movement of the fluid and the acoustic effect, and uses a simplified model for the flow, enabled noticeable improvements.

The method has been implemented for general 3D configurations and comparisons with analytic, another numerical method and measurements are provided. Complementary tests have to be conducted to catch the limitation of the potential flow assumption. However, now that the coupling has been carried out, and considering that the uniform flow assumption is reasonable far from the object, we can easily enrich the physics of the problem by considering more complex flows in the interior domain or other boundary conditions.

A Appendix

B Alternative computation of the coupling integral term I_M (11)

In the same fashion as the exterior problem, it is possible to transform the modal problem (39) to recover the classical Helmholtz equation by introducing a Prandtl–Glauert transformation associated to \mathbf{M}_M (this is the case in ACTIPOLE). In what follows, we note by $\widetilde{\cdot}^M$ the objects and operators transformed by the Prandtl–Glauert transformation associated to \mathbf{M}_M (normals, geometry, derivatives).

The waveguide is still supposed oriented along a local axis \mathbf{e}_{z_M} and with the uniform flow \mathbf{M}_M . As Γ_M is orthogonal to \mathbf{e}_{z_M} , we suppose $\widetilde{z_M|_{\Gamma_M}}^M = 0$. The flow \mathbf{M}_M is then parallel to \mathbf{e}_{z_M} .

In $\widetilde{\Omega}_M^M$, the transformed acoustic potential is decomposed into an incident and a diffracted potential: $\widetilde{\varphi}^M := \widetilde{\varphi}^{\text{inc}}^M + \widetilde{\varphi}^{\text{diff}}^M$, both satisfying

$$\widetilde{\Delta}^M \widetilde{\varphi}^{\text{inc,diff}}^M + \widetilde{k}_M^M \widetilde{\varphi}^{\text{inc,diff}}^M = 0, \quad \text{in } \widetilde{\Omega}_M^M. \quad (62)$$

The incident potential is known, whereas the diffracted potential is unknown. The following decomposition holds [38, 13]:

$$\begin{aligned} \widetilde{\varphi}^{\text{inc}}^M(\widetilde{x}^M, \widetilde{y}^M, \widetilde{z}^M) &= \sum_{(\iota)} \widetilde{\alpha}_\iota^M \widetilde{v}_\iota^M(\widetilde{x}^M, \widetilde{y}^M) \exp\left(i \widetilde{k}_\iota^+{}^M \widetilde{z}^M\right) \quad \text{in } \widetilde{\Omega}_M^M, \\ \widetilde{\varphi}^{\text{diff}}^M(\widetilde{x}^M, \widetilde{y}^M, \widetilde{z}^M) &= \sum_{(\iota)} \widetilde{\beta}_\iota^M \widetilde{v}_\iota^M(\widetilde{x}^M, \widetilde{y}^M) \exp\left(i \widetilde{k}_\iota^-{}^M \widetilde{z}^M\right) \quad \text{in } \widetilde{\Omega}_M^M, \end{aligned} \quad (63)$$

with ι a discrete index and where $\widetilde{\alpha}_\iota^M$ and $\widetilde{\beta}_\iota^M$ are the incident and diffracted modal coefficients. The basis functions \widetilde{v}_ι^M constitute an orthonormal modal basis function.

For instance for a cylindrical duct of radius R , ι corresponds to a couple of indices $(m, n) \in (\mathbb{Z} \times \mathbb{N}^*)$ and the functions \widetilde{v}_ι^M are defined in polar coordinates by [38, 13] by

$$\widetilde{v}_\iota^M(\widetilde{r}^M, \widetilde{\theta}^M) = \widetilde{v}_{m,n}^M(\widetilde{r}^M, \widetilde{\theta}^M) = \widetilde{V}_{m,n}^M J_m\left(\frac{r_{m,n}}{R} \widetilde{r}^M\right) \exp\left(i m \widetilde{\theta}^M\right), \quad (64)$$

with $r_{m,n}$ the n -th zero of the derivative of m -th Bessel function of the first kind J_m , $\widetilde{V}_{m,n}^M$ the normalization factor such that $\int_{\widetilde{\Gamma}_M^M} \widetilde{v}_\iota^M = 1$, and

$$\widetilde{k}_\iota^\pm{}^M = \widetilde{k}_{mn}^\pm{}^M = \pm \sqrt{\left(\widetilde{k}_M^M\right)^2 - \left(\frac{r_{m,n}}{R}\right)^2}, \quad \text{for propagating modes } (\widetilde{k}_{mn}^\pm{}^M \in \mathbb{R}), \quad (65)$$

$$\widetilde{k}_\iota^\pm{}^M = \widetilde{k}_{mn}^\pm{}^M = \pm i \sqrt{\left(\frac{r_{m,n}}{R}\right)^2 - \left(\widetilde{k}_M^M\right)^2}, \quad \text{for evanescent modes } (\widetilde{k}_{mn}^\pm{}^M \in \mathbb{C}). \quad (66)$$

Based on this decomposition, the expression of the Dirichlet-to-Neumann $\widetilde{\Lambda}_M^M$ operator is [10, 33]:

$$\widetilde{\nabla}^M \widetilde{\varphi}^M \cdot \widetilde{\mathbf{n}}^M = \widetilde{\Lambda}_M^M (\widetilde{\varphi}^M) := \sum_{(i)} \left(\widetilde{\alpha}_i^M \widetilde{Y}_i^+ + \widetilde{\beta}_i^M \widetilde{Y}_i^- \right) v_i \quad \text{on } \widetilde{\Gamma}_M^M, \quad (67)$$

with $\widetilde{Y}_i^\pm = -ik_i^\pm$. Similarly to Section 3.3, by using the Prandtl–Glauert transformation associated to \mathbf{M}_M , we infer

$$I_M(\varphi^i, \varphi^t) = -J_M \frac{\rho_M}{\rho_\infty} \int_{\widetilde{\Gamma}_M^M} \widetilde{\nabla}^M \widetilde{\varphi}^{iM} \cdot \widetilde{\mathbf{n}}^M \overline{\varphi}^{Mt} \quad (68)$$

$$= -J_M \frac{\rho_M}{\rho_\infty} \int_{\widetilde{\Gamma}_M^M} \widetilde{\Lambda}_M^M \left(\widetilde{\varphi}^{iM} \right) \overline{\varphi}^{Mt}. \quad (69)$$

Then, using the Dirichlet-to-Neumann operator (67), we obtain

$$I_M(\varphi^i, \varphi^t) = -J_M \frac{\rho_M}{\rho_\infty} \sum_{(i)} \left[\widetilde{\alpha}_i^M \widetilde{Y}_i^+ + \widetilde{\beta}_i^M \widetilde{Y}_i^- \right] \int_{\widetilde{\Gamma}_M^M} \widetilde{v}_i^M \overline{\varphi}^{Mt}. \quad (70)$$

However, to carry out a coupling between unknown functions written in the same variables, the integral I_M must be expressed in terms of quantities transformed by the Prandtl–Glauert transformation associated to \mathbf{M}_∞ . Using the results obtained in Section 3.3, we have that

$$J_M \int_{\widetilde{\Gamma}_M^M} \widetilde{g}^M(\widetilde{\mathbf{x}}^M) \overline{\widetilde{h}^M(\widetilde{\mathbf{x}}^M)} = \int_{\Gamma_M} \frac{1}{\widetilde{K}_M^M(\mathbf{x})} g(\mathbf{x}) \overline{h(\mathbf{x})} = \int_{\Gamma_M} \frac{J_\infty \widetilde{K}_\infty(\widetilde{\mathbf{x}})}{\widetilde{K}_M^M(\widetilde{\mathbf{x}})} \widetilde{g}(\widetilde{\mathbf{x}}) \overline{\widetilde{h}(\widetilde{\mathbf{x}})},$$

where \widetilde{K}_M^M and \widetilde{K}_∞ are defined in equation (26).

Equation (70) becomes

$$I_M(\varphi^i, \varphi^t) = -J_\infty \frac{\rho_M}{\rho_\infty} \sum_{(i)} \left[\widetilde{\alpha}_i^M \widetilde{Y}_i^+ + \widetilde{\beta}_i^M \widetilde{Y}_i^- \right] \int_{\Gamma_M} \frac{\widetilde{K}_\infty(\widetilde{\mathbf{x}})}{\widetilde{K}_M^M(\widetilde{\mathbf{x}})} \widetilde{v}_i \overline{\varphi}^t. \quad (71)$$

If \mathbf{M}_M and \mathbf{M}_∞ are colinear, there holds

$$\frac{\widetilde{K}_\infty}{\widetilde{K}_M^M} = \sqrt{\frac{1 - M_M^2}{1 - M_\infty^2}},$$

and otherwise, denoting $\alpha = \mathbf{M}_\infty \cdot \widetilde{\mathbf{n}}_M$,

$$\frac{\widetilde{K}_\infty}{\widetilde{K}_M^M} = \sqrt{\left[(1 + C_\infty \alpha^2)(1 + \widetilde{C}_M^M M_M^2) \right]^2 + C_\infty^2 \alpha^2 (M_\infty^2 - \alpha^2)}.$$

Acknowledgments

This work takes part in the AEROSON project, financed by the ANR (French National Research Agency). The authors would like to express their gratitude to Toufic Abboud (IMACS), Patrick Joly (INRIA) and Guillaume Sylvand (Airbus Group) for fruitful discussions and to Emilie Peynaud and François Madiot for their work during their internship at Airbus Group.

References

- [1] S. Abarbanel, D. Gottlieb, and J. S. Hesthaven. Well-posed perfectly matched layers for advective acoustics. *Journal of Computational Physics*, 154:266–283, 1999.

- [2] T. Abboud, P. Joly, J. Rodríguez, and I. Terrasse. Coupling discontinuous Galerkin methods and retarded potentials for transient wave propagation on unbounded domains. *Journal of Computational Physics*, 230:5877–5907, 2011.
- [3] P. R. Amestoy, I. S. Duff, J. Koster, and J.-Y. L’Excellent. A fully asynchronous multifrontal solver using distributed dynamic scheduling. *SIAM Journal on Matrix Analysis and Applications*, 23(1):15–41, 2001.
- [4] P. R. Amestoy, A. Guermouche, J.-Y. L’Excellent, and S. Pralet. Hybrid scheduling for the parallel solution of linear systems. *Parallel Computing*, 32(2):136–156, 2006.
- [5] R. Amiet and W. R. Sears. The aerodynamic noise of small-perturbation subsonic flows. *Journal of Fluid Mechanics*, 44:pp. 227–235, 1970.
- [6] R.J. Astley and J.G. Bain. A three-dimensional boundary element scheme for acoustic radiation in low mach number flows. *Journal of Sound and Vibration*, 109(3):445 – 465, 1986.
- [7] M. Beldi and F. S. Monastir. Resolution of the convected Helmholtz’s equation by integral equations. *The Journal of the Acoustical Society of America*, 103:2972, 1998.
- [8] J. P. Bérenger. A perfectly matched layer for the absorption of electromagnetic waves. *Journal of Computational Physics*, 114:185–200, 1994.
- [9] J. Bielak and R. C. Mac Camy. Symmetric Finite Element and Boundary Integral Coupling Methods for Fluid-Solid Interaction. *Quarterly of Applied Mathematics*, 49:107–119, 1991.
- [10] A.-S. Bonnet-Ben Dhia, L. Dahi, E. Luneville, and V. Pagneux. Acoustic diffraction by a plate in a uniform flow. *Mathematical Models and Methods in Applied Sciences*, 12(05):625–647, 2002.
- [11] A.-S. Bonnet-Ben Dhia, J.-F. Mercier, F. Millot, S. Pernet, and E. Peynaud. Time-Harmonic Acoustic Scattering in a Complex Flow: a Full Coupling Between Acoustics and Hydrodynamics. *Communications in Computational Physics*, 11(2):555–572, 2012.
- [12] E. J Brambley. Well-posed boundary condition for acoustic liners in straight ducts with flow. *AIAA journal*, 49(6):1272–1282, 2011.
- [13] M. Bruneau and T. Scelo. *Fundamentals of Acoustics*. ISTE, 2006.
- [14] A. J. Burton and G. F. Miller. The application of integral equation methods to the numerical solution of some exterior boundary-value problems. *Proceedings of the Royal Society of London. A. Mathematical and Physical Sciences*, 323(1553):201–210, 1971.
- [15] B. Carpentieri, I. S. Duff, L. Giraud, and G. Sylvand. Combining fast multipole techniques and an approximate inverse preconditioner for large electromagnetism calculations. *SIAM Journal on Scientific Computing*, 27:774–792, 2005.
- [16] F. Casenave, A. Ern, and G. Sylvand. Coupled BEM-FEM for the convected Helmholtz equation with non-uniform flow in a bounded domain. *Journal of Computational Physics*, 257, Part A(0):627–644, 2014.
- [17] C. J. Chapman. Similarity variables for sound radiation in a uniform flow. *Journal of Sound and Vibration*, 233(1):157 – 164, 2000.
- [18] P. G. Ciarlet. *The Finite Element Method for Elliptic Problems*. North Holland, Amsterdam, 1978.
- [19] M. Costabel. *Symmetric methods for the coupling of finite elements and boundary elements*. Fachbereich Mathematik. Technische Hochschule Darmstadt. Fachber., TH, 1987.

- [20] A. Craggs. An acoustic finite element approach for studying boundary flexibility and sound transmission between irregular enclosures. *Journal of Sound and Vibration*, 30:343–357, 1973.
- [21] A. Delnevo. Code ACTI3S harmonique : Justification Mathématique. Technical report, EADS CCR, 2001.
- [22] A. Delnevo. Code ACTI3S, Justifications Mathématiques : partie II, présence d’un écoulement uniforme. Technical report, EADS CCR, 2002.
- [23] A. Delnevo, S. Le Saint, G. Sylvand, and I. Terrasse. Numerical methods: Fast multipole method for shielding effects. *11th AIAA/CEAS Aeroacoustics Conference*, pages 2005–2971, 2005. Monterey.
- [24] Rolls-Royce Deutschland. Turbomachinery exhaust noise radiation experiments—part 1: Polar directivity measurements. 2008.
- [25] Rolls-Royce Deutschland. Turbomachinery exhaust noise radiation experiments—part 2: In-duct and far-field mode analysis. 2008.
- [26] F. Dubois, E. Duceau, F. Maréchal, and I. Terrasse. Lorentz transform and staggered finite differences for advective acoustics. Technical report, EADS and arXiv:1105.1458, 2002.
- [27] S. Duprey. *Analyse Mathématique et Numérique du Rayonnement Acoustique des Turboréacteurs*. PhD thesis, EADS-CRC ; Institut Elie Cartan-Université Poincaré Nancy, 2005.
- [28] W. Eversman. Approximation for thin boundary layers in the sheared flow duct transmission problem. *The Journal of the Acoustical Society of America*, 53(5):1346–1350, 1973.
- [29] L. Giraud, J. Langou, and G. Sylvand. On the parallel solution of large industrial wave propagation problems,. *Journal of Computational Acoustics*, 14:83–111, 2006.
- [30] H. Glauert. The effect of compressibility on the lift of an aerofoil. *Proceedings of the Royal Society of London. Series A, Containing Papers of a Mathematical and Physical Character*, 118(779):pp. 113–119, 1928.
- [31] F. H. Harlow, J. E. Welch, J. P. Shannon, and B. J. Daly. The MAC method. Technical report, Los Alamos Scientific Laboratory, march 1966.
- [32] C. Johnson and J. C. Nédélec. On the coupling of boundary integral and finite element methods. *Mathematics of Computation*, 35(152):1063–1079, 1980.
- [33] G. Legendre. *Rayonnement acoustique dans un fluide en écoulement : analyse mathématique et numérique de l’équation de Galbrun*. These, ENSTA ParisTech, September 2003.
- [34] V. Levillain. *Couplage éléments finis-équations intégrales pour la résolution des équations de Maxwell en milieu hétérogène*. PhD thesis, Thèse École Polytechnique, 1991.
- [35] S. Lidoine. *Approches théoriques du problème du rayonnement acoustique par une entrée d’air de turboréacteur: Comparaisons entre différentes méthodes analytiques et numériques*. PhD thesis, Ecole centrale de Lyon, 2002.
- [36] W.C.H. McLean. *Strongly Elliptic Systems and Boundary Integral Equations*. Cambridge University Press, 2000.
- [37] C.L. Morfey. Acoustic energy in non-uniform flows. *Journal of Sound and Vibration*, 14(2):159 – 170, 1971.
- [38] P. M. Morse and K. Ingard. *Theoretical acoustics*. McGraw-Hill Book Co., 1968.
- [39] A. Mosson, D. Binet, and J. Caprile. Simulation of the installation effects of the aircraft engine rear fan noise with ACTRAN/DGM. *20th AIAA/CEAS Aeroacoustics Conference*, 2014.

- [40] MK Myers. On the acoustic boundary condition in the presence of flow. *Journal of Sound and Vibration*, 71(3):429–434, 1980.
- [41] J.C. Nédélec. *Acoustic and Electromagnetic Equations: Integral Representations for Harmonic Problems*, volume 144 of *Applied Math. Sciences*. Springer, 2001.
- [42] J. Périaux. Three dimensional analysis of compressible potential flows with the finite element method. *International Journal for Numerical Methods in Engineering*, 9(4):775–831, 1975.
- [43] J. W. S. Rayleigh. *The theory of sound*. Macmillan and co, London, 1877.
- [44] V. Rokhlin. Rapid solution of integral equations of classical potential theory. *Journal of Computational Physics*, 60:187–207, 1985.
- [45] A. Hirschberg S. W. Rienstra. *An Introduction to Acoustics*. Eindhoven University of Technology, 2004.
- [46] H. A. Schenck. Improved Integral Formulation for Acoustic Radiation Problems. *The Journal of the Acoustical Society of America*, 44:41–58, 1968.
- [47] A. Sommerfeld. Die Greensche Funktionen der Schwingungsgleichung. *Jahresber. Deutsch. Math. Verein.*, 21:309–353, 1912.
- [48] G. Sylvand. *La méthode multipôle rapide en électromagnétisme. Performances, parallélisation, applications*. PhD thesis, Ecole des Ponts ParisTech, 2002.
- [49] A. Taflove. *Computational Electrodynamics: The Finite-Difference Time-Domain Method*. Artech House, Norwood, MA, 1995.
- [50] J. Virieux. PSV-wave propagation in heterogeneous media: velocity-stress finite difference method. *Geophysics*, 51:889–901, 1986.
- [51] M.C.M. Wright. *Lecture Notes On The Mathematics Of Acoustics*. Imperial College Press, 2005.
- [52] F. Zhang. *The Schur Complement and Its Applications*. Numerical Methods and Algorithms. Springer, 2005.
- [53] O. C. Zienkiewicz, D. W. Kelly, and P. Bettess. The coupling of the finite element method and boundary solution procedures. *International Journal for Numerical Methods in Engineering*, 11:355–375, 1977.